BIOCHEMISTRY
including biophysical chemistry & molecular biology

Article

pubs.acs.org/biochemistry

# Sulfiredoxin Redox-Sensitive Interaction with S100A4 and Non-Muscle Myosin IIA Regulates Cancer Cell Motility

Robert R. Bowers,[†] Yefim Manevich,[†] Danyelle M. Townsend,[‡] and Kenneth D. Tew*[,†]

[†]Department of Cell and Molecular Pharmacology and Experimental Therapeutics, Medical University of South Carolina, 173 Ashley Avenue, Charleston, South Carolina 29425, United States

[‡]Department of Pharmaceutical and Biomedical Sciences, Medical University of South Carolina, 173 Ashley Avenue, Charleston, South Carolina 29425, United States

**ABSTRACT:** Sulfiredoxin (Srx) is a redox active protein that participates in the reduction of oxidized cysteine residues. Here we identify a novel function of Srx through its specific binding to S-glutathionylated S100A4 affecting its interaction with non-muscle myosin (NMIIA), thereby modulating the effect of S100A4 on NMIIA function and impacting cell adhesion and migration. Srx forms a complex with S100A4 (and has stronger affinity for S-glutathionylated S100A4), regulates its activity, and mediates redox regulation of the interaction of S100A4 with NMIIA. The consequence of this regulation is microfilament remodeling and altered cellular motility and adhesion. Srx-overexpressing cells had reduced levels of adhesion, decreased levels of Tyr[397]-phosphorylated focal adhesion kinase, and increased cell motility in wound healing assays. These results describe a novel redox-sensitive role for Srx in mediating complex protein interactions with plausible consequences for cancer cell motility.

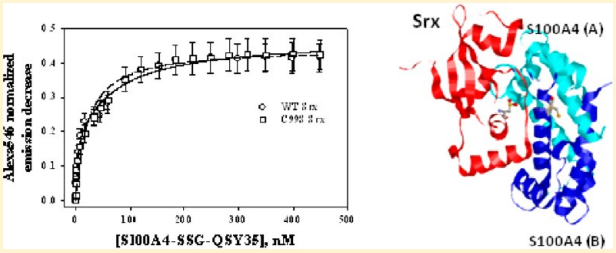


Redox homeostasis is critical for normal physiology, and excessive reactive oxygen species are associated with a number of human diseases, including cancer. Thiol groups in proteins are among the most reactive amino acid side chains and are subject to oxidative post-translational modifications such as disulfide bonds (S−S), sulfenic (SOH), sulfinic ($SO_2H$), and sulfonic ($SO_3H$) acids, and S-nitrosylation (SNO). In addition, mixed disulfides of protein thiols and glutathione can result from the S-glutathionylation (PS−SG) of low-p$K_a$ cysteine residues in certain target proteins. These oxidative cysteine modifications alter the structure and function of a variety of proteins and are involved in cell signaling.[1] Sulfiredoxin (Srx) is a ubiquitous antioxidant protein with tissue specific expression patterns and elevated levels in a number of human cancers.[2] Initial indications are that Srx1 null mice have no obvious phenotype other than increased sensitivity to lipopolysaccharide-induced endotoxic shock[3] and increased sensitivity to ethanol-induced oxidative toxicity in liver.[4] Srx was originally identified as a $Mg^{2+}$ATP-dependent sulfinic acid reductase specific to 2-Cys peroxiredoxins (Prxs), where it catalyzes reactivation of hyperoxidized (sulfinic acid) Prxs,[5−7] but a few studies have shown that Srx possesses deglutathionylating activity toward actin, PTP1B, and PrxI.[5,8,9]

Even in the absence of a precise mechanism(s), Srx expression has been linked with both cell division and tumorigenicity.[2,9] In this study, we sought to address this connection by identifying binding partners of Srx. We identified several novel candidate proteins that co-immunoprecipitated with Srx. Among these, the heavy chain of non-muscle myosin IIA (NMIIA) is in a position downstream of convergent signaling pathways central to cell adhesion, migration, and microfilament architecture.[10] In addition, Srx was also found to co-immunoprecipitate with S100A4, a calcium binding protein that plays a key role in regulating NMIIA activity.[11] These observations led us to consider whether Srx may be involved in some aspect of regulation of cell migration. Cell migration is typically viewed as a series of coordinated steps. Initially, either broad (lamellipodia) or spikelike (filopodia) protrusions of the membrane, or both, extend in the direction of migration. These membrane extensions are driven by polymerization of actin filaments and stabilized by nascent cell adhesions that link the underlying extracellular matrix to the actin cytoskeleton. Actomyosin-based contractions provide the force necessary to generate traction and to initiate detachment of adhesions at the rear of the cell. Rho family GTPases and their targets, especially tyrosine kinases, regulate the dynamics of focal complexes and actomyosin filaments.[12] Moreover, ROS and redox conditions influence the actomyosin complex. For example, NOX family enzymes are linked to invasion and metastasis.[13,14] NOX-generated superoxide anion radicals can spontaneously dismutate into $H_2O_2$, facilitating interaction with NO (with $NOOO^-$ generation) and subsequent nitrosation of protein cysteines. In the presence of high levels of GSH in the cytosol (2−10 mM), S-nitrosylated cysteines can be rapidly converted to S-glutathionylated residues, and these directly influence actin−myosin interactions and the polymerization state of actin.[15−17] Srx may participate in deglutathionylation of actin,[8]

**Received:** December 13, 2011
**Revised:** August 29, 2012
**Published:** August 30, 2012

   dx.doi.org/10.1021/bi301006w | *Biochemistry* 2012, 51, 7740−7754

providing a redox-mediated mechanism for regulating actin polymerization.

There are more than 20 S100 proteins in the human genome. They are low-molecular mass proteins with conserved structural motifs of two EF-hand $Ca^{2+}$-binding domains connected by a variable hinge region.[18] Specific S100s can regulate calcium homeostasis, cytoskeletal rearrangements, cell proliferation, and apoptosis. Calcium binding causing S100 structural rearrangements can expose hydrophobic residues and result in $Ca^{2+}$-dependent interactions with target proteins.[19] Cysteine residues within S100 homologues are highly conserved between species and are subject to S-glutathionylation.[20−22] S100A4 is a metastasis-associated $Ca^{2+}$-binding protein found in aggressive tumors that interacts with the tail region of NMIIA, preventing filament formation and promoting the disassembly of filaments resulting in enhanced cell migration.[23,24] Recent reports identify a critical role for Cys81 of S100A4 in regulating its interaction with NMIIA.[25]

In this study, we identified S100A4 and NMIIA as part of a protein complex with Srx. In vitro FRET-based analyses demonstrated tight binding (low nanomolar $K_D$) of Srx and S100A4. Further, the catalytic Cys99 of Srx was shown to be involved in this binding, and S-glutathionylation of S100A4 markedly strengthened the Srx−S100A4 interaction, observations consistent with redox regulation of the Srx−S100A4 interaction. Oxidative stress strengthened the interaction of Srx with both NMIIA and S100A4. In addition, we found that Srx expression levels have a marked effect on cell adhesion, actin microfilament architecture, and cell migration, likely as a consequence of Srx-mediated redox regulation of S100A4−NMIIA interactions. There are implications for these data that involve Srx and this protein complex in cancer cell migration and metastasis.

## EXPERIMENTAL PROCEDURES

**Reagents.** General chemicals and FLAG immunoprecipitation kits were from Sigma (St. Louis, MO). Dulbecco's Modified Eagle Medium (DMEM)/Ham's F12 mix (50/50) was obtained from Mediatech Inc. (Manassas, VA). A monoclonal antibody against human sulfiredoxin was produced in the Medical University of South Carolina core facility as described previously.[9] The monoclonal antibody against S-glutathionylated protein was purchased from Virogen (Watertown, MA). Rabbit polyclonal antibodies to non-muscle myosin IIA (ab24762) and S100A4 (ab41532) were from Abcam (Cambridge, MA). Rabbit polyclonal antibodies against focal adhesion kinase (FAK) (catalog no. 3285) and phospho-FAK (catalog no. 3283) were from Cell Signaling Technology (Danvers, MA). Rhodamine Red-X-conjugated donkey anti-rabbit and horseradish peroxidase-conjugated donkey anti-rabbit and anti-mouse secondary antibodies were from Jackson ImmunoResearch (West Grove, PA). CNBr-activated Sepharose was obtained from GE Healthcare (Piscataway, NJ). Oregon Green 488 phalloidin and Prolong Gold antifade reagent with DAPI were from Invitrogen (Carlsbad, CA). Alexa546 *N*-succinimidyl ester and QSY35 acetic acid succinimidyl ester were from Invitrogen. PABA/NO was provided by L. Keefer (National Cancer Institute, Frederick, MD).[26] Recombinant human S100A4 protein was from R&D Systems (Minneapolis, MN). Lab-Tek II Chamber Slides were obtained from Nalge Nunc International (Rochester, NY).

**Cell Culture.** Non-small cell lung cancer-derived A549 cells (American Type Culture Collection, Manassas, VA) were maintained in DMEM/F12 mix (50/50) containing 10% fetal bovine serum (FBS). A549 cells expressing FLAG-tagged Srx were as described previously.[9] Knockdown of sulfiredoxin expression by shRNA retroviral gene transfer was accomplished using the pLK01.1 vector and 1.2 mg/mL puromycin selection according to the protocol of the manufacturer (Clontech Laboratories, Inc., Mountain View, CA). Nitrosative stress in WT, KD, and OE A549 cells was induced by the addition of PABA/NO (20 $\mu$M) to cell monolayers in complete media. After incubation for 20 min at 37 °C, cells were washed three times with ice-cold PBS and lysed with Triton lysis buffer.[27] The supernatants of control and treated cell lysates (14000*g* for 10 min) were used for protein concentration analyses (Bradford) and electrophoretic resolution of the proteins by sodium dodecyl sulfate−polyacrylamide gel electrophoresis (SDS−PAGE).

**Immunoblot and Immunoprecipitation.** Cells were washed with ice-cold phosphate-buffered saline (PBS) and lysed in Triton lysis buffer. Immunoprecipitation of FLAG-tagged Srx was achieved using the FLAG immunoprecipitation kit according to the protocol of the manufacturer (Sigma). For immunoprecipitation of NMIIA, primary antibodies were conjugated to cyanogen bromide-activated Sepharose according to the manufacturer's recommendations (GE Healthcare). Cell lysates (~1 mg of total protein) were incubated with a Sepharose-conjugated antibody overnight at 4 °C under constant agitation. The Sepharose immunoprecipitate was separated by centrifugation (14000*g* for 5 min). After being washed three times with PBS, the precipitated proteins were separated from the Sepharose-conjugated antibody by acidification with glycine buffer (0.5 M, pH 2.1, containing 150 mM NaCl) and collected by centrifugation (14000*g* for 15 min at 4 °C). Cell lysates and immunoprecipitates were resolved by 12% SDS−PAGE and transferred onto PVDF membranes (Bio-Rad, Hercules, CA). Nonspecific binding was blocked by incubating membranes in TBST (Tris-buffered saline with 0.1% Tween 20) containing 5% nonfat dry milk or 5% bovine serum albumin fraction V. Primary antibodies were incubated for 2 h at room temperature or at 4 °C overnight, and secondary HRP-conjugated antibodies were incubated for 1−2 h at room temperature. The blots were developed with ECL (GE Healthcare Bio-Sciences Corp.). The blots were scanned with a Bio-Rad ChemiDoc system and visualized with a trans-illuminator.

**Liquid Chromatography Coupled to Electrospray Ionization Tandem Mass Spectrometry.** Immunoprecipitated samples were treated with 9 volumes of cold acetone. The pellet was then redissolved with Rapigest (Waters, Milford, MA), and the manufacturer's protocol was followed for trypsin digestion. Trypsin-digested samples were analyzed via liquid chromatography (LC)−electrospray ionization (ESI) tandem mass spectrometry (MS/MS) on a linear ion trap mass spectrometer (LTQ, Thermo Finnigan) coupled to an LC Packings nano LC system. A C-18 reversed phase LC column (packed in house, 15 cm, 75 $\mu$m inner diameter, particle size of 5 $\mu$m) was eluted with a linear 60 min gradient from 2% acetonitrile and 0.1% formic acid to 60% acetonitrile and 0.1% formic acid. A blank injection was analyzed between samples to limit carryover. Data Dependent Analysis was utilized on the LTQ to perform MS/MS on the 10 most intense ions in each MS spectrum with a minimum ion count of 1000. Dynamic Exclusion was set to exclude ions from MS/MS selection for 3 min after being selected twice in a 30 s window. The MS/MS

data were searched against the human database (http://www.ncbi.nlm.nih.gov/protein) utilizing Thermo Finnigan Bioworks version 3.3.1. Variable modifications of methionine oxidation, carboxamidomethylation of cysteines, and phosphorylation of serine, threonine, and tyrosine were considered. Protein identifications must meet the minimal criteria of a Protein Probability of $1.0 \times 10^{-3}$ or better and have Xcorr versus charge state values of >1.5, 2.0, and 2.5 for +1, +2, and +3 ions, respectively, with at least two unique peptides matching the protein, and a good match for at least four consecutive y or b ion series from the MS/MS spectra.

**Molecular Modeling of the Interaction of Srx with S100A4.** Modeling of binary protein interactions was performed using ZDOCK software (http://zdock.bu.edu) without any restriction of individual protein structural elements or sequences. Only models with the highest probability score were selected for further analysis. The crystal structures of human Srx [Protein Data Bank (PDB) entry 1XW3, in complex with ADP] and S100A4 (PDB entry 3CGA) were used for modeling. Individual protein structure and binary models were visualized using RasMol (version 2.7.5, http://www.bernstein-plus-sons.com/software/rasmol/doc/rasmol.html).

**Interaction of Sulfiredoxin with S100A4.** Purified Srx (C99S) protein was incubated with a 5-fold excess of succinimidyl ester of Alexa546 Fluor carboxylic acid (Invitrogen), and S100A4 (S100A4-SSG)-purified protein was incubated with a 5-fold excess of succinimidyl ester of QSY35 acetic acid (Invitrogen) at room temperature, overnight, under constant agitation to label primary amines according to the manufacturer's recommendations. The reaction mixture was processed using a BioSpin 6 (Bio-Rad) size-exclusion spin column to remove an excess of unreacted dyes and exchange reaction buffers to 20 mM PB (pH 7.4). Spectroscopic analysis of Alexa546 Fluor label incorporation indicated ~2.0 mol of dye/mol of Srx or C99S mutant monomer. In vitro S-glutathionylation of S100A4 [25 $\mu$g in 1.0 mL of 10 mM PB (pH 7.4)] was performed with 50 $\mu$M PABA/NO and 1 mM GSH (room temperature, 1 h, under constant stirring) using procedures previously described.[28] We designed the high-performance liquid chromatography (HPLC) analysis, which allowed us to monitor all reactants simultaneously. HPLC was performed with a Binary HPLC Pumps 1525 separation unit, a model 2487 dual $\lambda$ absorbance detector, and a 717plus autosampler (all from Waters). We used a $C_{18}$ column [4.6 mm × 150 mm, 5 $\mu$m particle size, and 100 Å pore size (SunFire, Waters)] and isocratic elution (1 mL/min) with a 45/55 (v/v) mixture of $H_2O$ with 0.1% TFA and ACN with 0.1% TFA and detection at 220 nm. Chromatography and data processing were performed using Empower 2 Chromatography software (Waters). The data are representive of three independent experiments.

The reaction mixture was processed using a BioSpin 6 size-exclusion microcolumn to eliminate excess reagents and resulted in essentially homogeneous (>98% pure) S-glutathinylated S100A4. Resultant S-glutathionylated proteins were detected by Western blotting with anti-glutathionylated antibodies (Virogen, Watertown, MA). Intact and S-glutathionylated S100A4 were used for fluorescent labeling with the succinimidyl ester of QSY35 acetic acid. Spectroscopic analysis of QSY35 label incorporation showed ~3.0 mol of dye/mol of S100A4 or S100A4-SSG protein monomers.

Concentrations of all proteins were determined spectroscopically: Srx and C99S mutant using an $\varepsilon$ of 7280 $M^{-1}$ $cm^{-1}$ at 280 nm,[29] Alexa546-labeled Srx (C99S) using a correction coefficient of 0.12 for the label absorbance ($\varepsilon$ = 104000 $M^{-1}$ $cm^{-1}$ at 554 nm) at 280 nm, S100A4 (S100A4-SSG) using an $\varepsilon$ of 3040 $M^{-1}$ $cm^{-1}$ [23] at 280 nm, and S100A4 (S100A4-SSG) labeled with QSY35 using a correction coefficient of 0.23 for the label absorbance ($\varepsilon$ = 24000 $M^{-1}$ $cm^{-1}$ at 490 nm) at 280 nm.

The fluorescence analysis of FRET-based ($R_0$ = 25 Å for the Alexa546-QSY35 couple) protein binding was performed using the QM-4 spectrofluorometer (PTI, Birmingham, NJ). We used 1.0 or 2.0 nM Alexa546-labeled hSrx(C99S) in 10 mM PB (pH 7.4) for our titration experiments. Titration was performed in a 5 mm × 5 mm × 40 mm quartz cuvette in a fluorometer sample holder at room temperature. Emission spectra of Alexa546-labeled Srx (C99S) were recorded (excitation at 546 nm) before any additions. Because of the higher accuracy of measurements at low protein concentrations, we used integration of the emission spectra as a measure of the FRET effect on the "donor" (Alexa546) fluorescence. The indicated amounts (0.5−400 nM) of QSY35-labeled S100A4 were added to 2.0 nM Alexa546-labeled Srx(C99S) in solution. After incubation for ~5 min under constant shaking to reach equilibrium between "free" and "bound" S100A4, the emission spectra of Alexa546 with the indicated concentrations of S100A4-QSY35 were recorded. The effect of each S100A4-QSY35 concentration was measured individually. To eliminate any variation in actual concentrations of Srx(C99S), any differences between the integration of the latter and the initial Alexa546 spectra were normalized to the integral of the initial emission spectra. Similarly, the indicated amounts (0.2−250 nM) of S100A4-SSG-QSY35 were added to 1.0 nM Alexa546-labeled Srx(C99S) in solution. All experimental details were the same as for titration with S100A4-QSY35. The results were corrected for an effect of sample dilution. The *Y*-axis of the graphic representation of experimental data corresponds with the decrease in Alexa546 emission, which is proportional to amount of S100A4(S100A4-SSG)-QSY35 bound to Srx(C99S). The *X*-axis represents a total amount of added S100A4 or S100A4-SSG labeled with QSY35. Each titration point was determined in triplicate and is presented as the mean ± the standard deviation (SD).

The experimental data for binding of S100A4 to Srx(C99S) were processed using a "one-site saturation model" (Pharmacology application, SigmaPlot 10.0, SyStat) with the best hyperbolic fit ($R^2 \geq 0.99$) according to equation for one binding site:

$$Y = B_{max1}X/(K_{D1} + X) \quad (1)$$

where *X* is the concentration of added S100A4 protein, *Y* is the normalized decrease in Alexa546 fluorescence corresponding to the specific binding of S100A4, and $B_{max1}$ is the saturated number of binding complexes with apparent equilibrium dissociation constant $K_{D1}$.

The experimental data for binding of S100A4-SSG to Srx(C99S) were processed using a "two-site saturation model" (Pharmacology application, SigmaPlot 10.0, SyStat) with the best hyperbolic fit ($R^2 \geq 0.99$) according to the equation for two binding sites with different affinities:

$$Y = B_{max1}X/(K_{D1} + X) + B_{max2}X/(K_{D2} + X) \quad (2)$$

where *X* is the concentration of added S100A4 (S100A4SSG) protein, *Y* is the normalized decrease in Alexa546 fluorescence corresponding to the specific binding of S100A4, $B_{max1}$ is the

saturated number of high-affinity binding complexes with apparent equilibrium dissociation constant $K_{D1}$, and $B_{max2}$ is the saturated number of lower-affinity binding complexes with apparent equilibrium dissociation constant $K_{D2}$.

Competition experiments were used to determine what effect (if any) Srx or Srx(C99S) fluorescent labeling had on the specificity of its binding to S100A4. We used 2 nM Srx or Srx(C99S)-Alexa546 for these experiments. At each point of titration, an emission spectrum of Alexa546 was recorded before and after incubation with an indicated amount of S100A4-QSY35 for 5 min. Following this, 2.0 nM unlabeled Srx or Srx(C99S) was added, and after incubation at room temperature for 5 min, the emission spectra of Alexa546 were recorded. In parallel experiments, a 2.0 nM solution of Srx or Srx(C99S)-Alexa546 was added and emission spectra were recorded. All emission spectra were integrated and used to generate the titration curves according to the formula

$$E = (\int_{INT} - \int_{S100A4})/\int_{INT} \quad (3)$$

where $E$ is the normalized decrease in Alexa546 emission caused by the S100A4-QSY35 binding-mediated FRET, $\int_{INT}$ corresponds to the integration of Alexa546-labeled or unlabeled mixed with intact Srx(C99S) protein emission spectra, and $\int_{S100A4}$ corresponds to the integration of emission spectra of Alexa546-labeled or mixed protein with intact Srx(C99S) after incubation with the indicated amounts of S100A4-QSY35. All spectra were corrected for trivial dilution effects.

To determine if S100A4 fluorescent labeling with QSY35 altered the specificity of its binding to Srx(C99S), we used "back-titrations" with intact unlabeled S100A4 protein. After addition of 150.0 nM S100A4-QSY35 to 2.0 nM Srx or Srx(C99S)-Alexa546 and incubation for 5 min at room temperature, the indicated amounts of intact unlabeled S100A4 were added and incubated for an additional 5 min at room temperature under constant stirring. The emission spectra of 2.0 nM Srx- or Srx(C99S)-Alexa546 before and after incubation with 150.0 nM S100A4-QSY35 were recorded. Similarly, the emission spectra of 2.0 nM Srx- or Srx(C99S)-Alexa546 after incubation with 150.0 nM S100A4-QSY35 and addition of indicated amounts of intact unlabeled S100A4 were recorded. All emission spectra were corrected for trivial dilution effects, integrated, and used for generation of back-titration curves according to the formula

$$E = [\int_{INT} - \int_{S100A4(SAT+UL)}]/\int_{INT} \quad (4)$$

where $E$ is the normalized decrease in Alexa546 emission caused by the S100A4-QSY35 binding-mediated FRET, $\int_{INT}$ corresponds to the integration of Srx(C99S)-Alexa546 (2.0 nM) emission spectra, and $\int_{S100A4(SAT+UL)}$ corresponds to the integration of emission spectra after addition of 150 nM S100A4-QSY35 and the indicated concentrations of intact unlabeled S100A4.

The results of competition between Alexa546-labeled and unlabeled intact Srx or Srx(C99S) binding of QSY35-labeled S100A4 were analyzed using the standard (as above) SigmaPlot pharmacological application, and one-site saturation model (SigmaPlot 10.0). The latter showed the best fit for the experimental data ($R^2 \geq 0.98$). The results of the analysis are presented in Figure 6 (panels A and B) as means ± SD for three independent experiments.

To determine what influence, if any, the QSY35 labeling of S100A4 has on its binding to Srx(C99S) (mean ± SD for three independent experiments), we determined binding isotherms of the back-titration experiments (Figure 6C). The same experimental data presented as an increase in Alexa546 fluorescence (as a result of a decreased level of quenching) after titration with increasing amounts of intact S100A4 were used to calculate an intrinsic equilibrium $K_D$ for the Srx− or Srx(C99S)−Alexa546−S100A4 complex using a hyperbolic fit and a standard SigmaPlot pharmacological application (SigmaPlot 10.0).

**CD Analysis.** rhS100A4 (100 μM) was analyzed in 10 mM PB (pH 7.4) before and after S-glutathionylation (1 mM GSH and 50 μM PABA/NO for 1 h at room temperature; excess of reagents removed by BioSpin 6 micro filtration) in 2 mm × 10 mm × 40 mm quartz cuvettes in a CD spectrometer (model 420, AVIV, Lakewood, NJ) at 22 °C in the far-UV region (180−260 nm) with a step size of 0.5 nm and averaging of two repeats. The effects of $Ca^{2+}$ were evaluated by addition of 150 μM $CaCl_2$ or 2.0 mM EGTA. Actual CD data were recalculated as molecular ellipticity units according to protein concentration and amino acid content. The background of all used reagents was subtracted from final spectra.

**Fluorescent Imaging of Actin Microfilaments and Focal Adhesions.** For visualizing actin microfilaments and focal adhesions in spreading cells, $2 \times 10^3$ cells were seeded onto four-well Lab-TekTM II Chamber Slides that were previously coated with 10 μg/mL human fibronectin. After being allowed to adhere overnight, cells were fixed with 4% paraformaldehyde for 30 min. Cells were permeabilized by a 20 min incubation in 0.2% Triton X-100 in PBS. Nonspecific protein binding was blocked by incubating the cells with 1% bovine serum albumin (BSA) in PBS for 20 min. Cells were then incubated for 1 h in the primary anti-phospho-FAK antibody diluted 1/100 in 1% BSA in PBS. After the unbound primary antibody had been washed away with three rinses of PBS containing 0.05% Tween 20, cells were incubated with Rhodamine Red-X-conjugated secondary antibody and Oregon Green 488-conjugated phalloidin. Labeled cells were imaged by fluorescence microscopy [Nikon eclipse E800 camera (Nikon Instruments, Inc., Lewisville, TX) with Nikon DS-U1 version 5.03 (Photometrics, Tucson, AZ)].

**Cell Adhesion, Globular and Filamentous Actin, and Migration Assays.** For cell adhesion assays, $1 \times 10^5$ cells were seeded onto 24-well cell culture dishes that had been coated with 5 μg of fibronectin or heat-denatured bovine serum albumin (BSA). After the cells had been allowed to adhere for 2 h, cells that had not adhered were removed by gently rinsing the wells with PBS three times. The adherent cells were fixed with 4% paraformaldehyde and stained with crystal violet. The crystal violet was solubilized with 0.1 M acetic acid, and the absorbance at 570 nm was read. The number of cells that adhered to BSA was negligible. For determining the ratio of globular (G) to filamentous (F) actin, cells were lysed in buffer containing 1% Triton X-100. Under these conditions, F actin remains insoluble and was separated from G actin by centrifugation at 16000*g*. The pellets containing F actin were resuspended in Laemmli sample buffer by being passed through a 20 gauge needle and sonication. Equal amounts of supernatants and pellets were resolved by SDS−PAGE. For wound healing assays, $1 \times 10^6$ cells were seeded onto 3.5 cm dishes. The next day cell monolayers were wounded with a 200 μL pipet tip, and 4-fold magnified images were acquired after


dx.doi.org/10.1021/bi301006w | *Biochemistry* 2012, 51, 7740−7754

**Table 1. MS Identification of the Srx Binding Partners Identified by Co-Immunoprecipitation in A549 Cells**

| protein | molecular mass (Da) | no. of unique peptides | protein probability | XC score of protein | NCBI accession number |
|---|---|---|---|---|---|
| sulfiredoxin 1 homologue | 14250.4 | 7 | $8.84 \times 10^{-7}$ | 80.21 | 22129778 |
| protein phosphatase 1B isoform 2 | 42743.8 | 2 | $7.16 \times 10^{-4}$ | 28.12 | 29558022 |
| peroxiredoxin III isoform b | 25822.3 | 2 | $3.62 \times 10^{-9}$ | 20.23 | 32483377 |
| thioredoxin peroxidase (peroxiredoxin IV) | 30520.8 | 2 | $2.31 \times 10^{-8}$ | 20.15 | 5453549 |
| calmodulin-like 5 | 15882.8 | 2 | $5.21 \times 10^{-6}$ | 20.15 | 55859601 |
| serine protease 3 (hCG22067 or PRSS3) | 29691.7 | 2 | $1.51 \times 10^{-4}$ | 24.11 | 119572363 |
| kinesin family member 11 (Eg5) | 119084.9 | 5 | $3.74 \times 10^{-7}$ | 50.21 | 13699824 |
| myosin; heavy polypeptide 9, non-muscle | 226390.6 | 7 | $1.07 \times 10^{-5}$ | 70.25 | 12667788 |

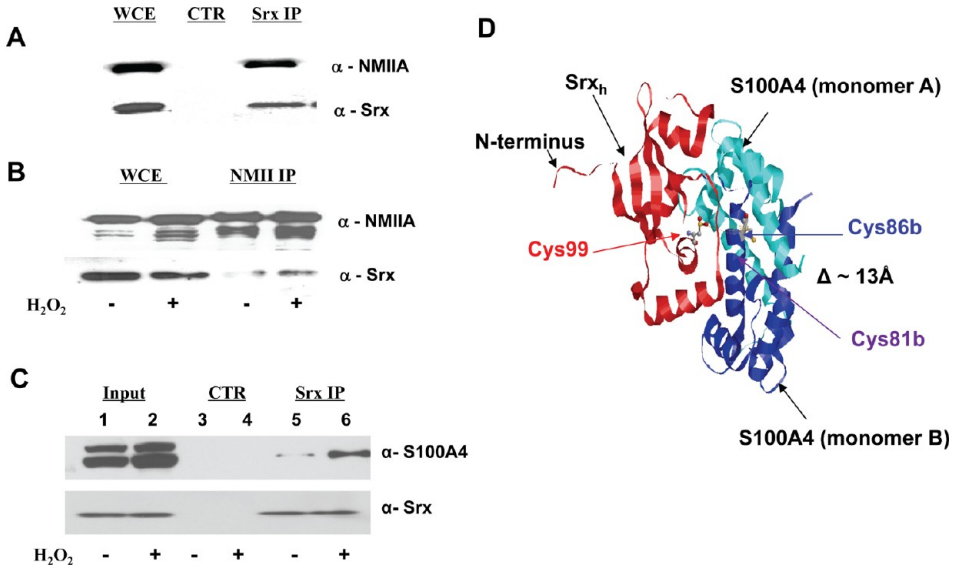


**Figure 1.** Srx with NMIIA and Srx with S100A4 co-immunoprecipitate in A549 cells. (A) FLAG-tagged Srx was immunoprecipitated from A549 cells as described in Experimental Procedures. Whole cell extract (WCE), immunoprecipitation control (CTR), and Srx immunoprecipitates (Srx IP) were resolved by SDS−PAGE and immunoblotted with antibodies against NMIIA and Srx. (B) NMIIA was immunoprecipitated from A549 cells treated (or not) with 200 $\mu$M $H_2O_2$ for 20 min, and after SDS−PAGE, whole cell extracts and NMIIA immunoprecipitates were immunoblotted with antibodies against NMIIA and Srx. (C) Sulfiredoxin was immunoprecipitated from A549 cells treated (or not) with 200 $\mu$M $H_2O_2$ for 20 min. Whole cell extracts (input), IgG control (Control), and Srx immunoprecipitates (Srx IP) were resolved by SDS−PAGE and immunoblotted with antibodies against S100A4 or Srx. (D) Structure of the S100A4−Srx complex (ZDOCK). Monomers of S100A4 are colored blue and light blue, and Srx is colored red. Cysteine residues of both proteins are presented as "balls and sticks" using CPK color code. The complex was visualized using RasMol (version 2.7.5).

24 h. Three independent measurements using ImageJ version 1.45 (http://rsbweb.nih.gov/ij/download.html) were used to quantify cell migration.

**Statistical Analysis of Experimental Data.** All experimental data were statistically evaluated using SigmaStat 3.5 (Systat Software Inc., San Jose, CA) and represented as means ± SD. Analysis of variance (ANOVA) was used to evaluate the significance of differences between control and treatment groups.

## RESULTS

**Immunoprecipitation of Sulfiredoxin Reveals Novel Binding Partners.** To identify binding partners of Srx, FLAG-tagged Srx was immunoprecipitated from A549 cells and resultant proteins were identified by LC−ESI-MS/MS. Lysates from control cells transfected with the empty FLAG vector were used to control for nonspecific binding of proteins to the FLAG affinity resin. After these proteins, and keratins and immunoglobulins, had been excluded, eight proteins were identified (Table 1). As expected, Srx itself was detected in the immunoprecipitates from A549 cells expressing FLAG-tagged Srx but not in the vector only controls. Protein tyrosine phosphatase 1B (PTP1B[9]), PrxIII, and PrxIV[6] have been identified as Srx binding partners, and their detection validated the reliability of the method. Four proteins not previously reported to interact either directly or indirectly with Srx were identified. Of these, kinesin family member 11 (KIF11or Eg5) is implicated in spindle movement prior to, and during, anaphase,[30] and its expression correlates with the response of non-small cell lung cancer to drugs.[31] Other reports link the protein with the transport of vesicles from the Golgi apparatus to the endoplasmic reticulum.[32] Silencing of serine protease 3 (PRSS3) has been suggested as a putative tumor suppressor gene in non-small cell lung cancer.[33] Furthermore, serine protease inhibitors are regulated by reversible S-glutathionylation,[34] providing a putative connection with Srx-mediated regulation of redox status for this complex of protease and protease inhibitor. Calmodulin-like protein 5 binds $Ca^{2+}$ with high affinity,[35] and we have found that S-glutathionylation of eNOS[27] is directly linked with increases in $Ca^{2+}$ flux and calmodulin activation levels. These observations are consistent with the involvement of Srx with $Ca^{2+}$ pathways.

In context with the cell motility studies, the association between Srx and NMIIA heavy chain polypeptide 9 was studied


dx.doi.org/10.1021/bi301006w | Biochemistry 2012, 51, 7740−7754

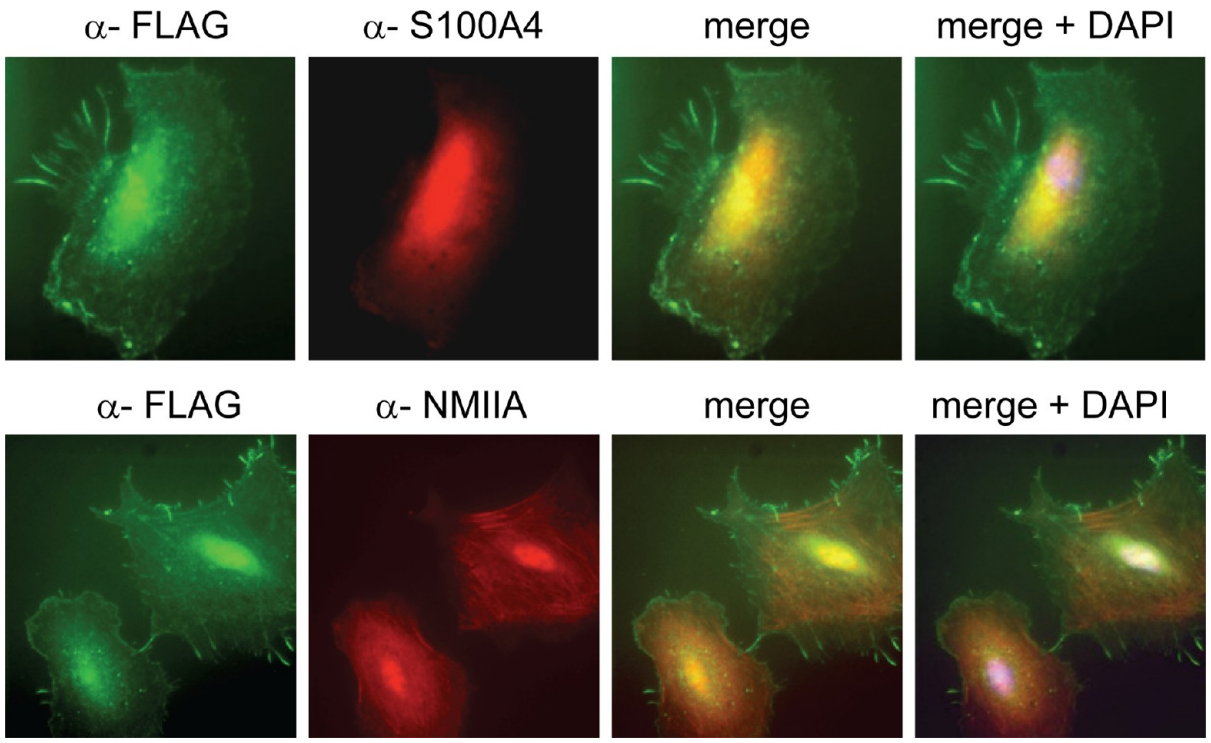


**Figure 2.** Immunocytochemistry reveals colocalization of Srx and S100A4 or Srx and NMIIA in A549 cells. Immunofluorescent images from A549 cells were acquired using anti-FLAG primary antibodies and FITC-conjugated secondary antibodies to detect FLAG-tagged Srx and anti-S100A4 or anti-NMIIA primary antibodies and rhodamine-conjugated secondary antibodies. Nuclei were stained with DAPI.

in more detail. Moreover, although in this experiment S100A4 was not identified as an Srx binding partner, it should be noted that the method is not exhaustive, and in our study, the Srx:S100A4 interaction was confirmed by in vitro FRET-based studies and subsequent co-immunoprecipitation analyses.

**Interaction of Srx with NMIIA and S100A4.** To confirm intracellular binding of Srx to NMIIA, we repeated the immunoprecipitation of FLAG-tagged Srx from A549 cells and detected NMIIA protein by immunoblotting (Figure 1A). Lysates from control cells transfected with the empty FLAG vector were used as a control for nonspecific binding of proteins to the FLAG affinity resin. Further, immunoprecipitation of NMIIA from wild-type (WT) A549 cells followed by immunoblotting for Srx confirmed the interaction of NMIIA and Srx in A549 cells expressing endogenous Srx, demonstrating the Srx−NMIIA interaction is not an artifact of Srx overexpression [Srx OE (Figure 1B)]. Increasing the level of oxidative stress with $H_2O_2$ increased the amount of Srx that interacted with NMIIA. As a consequence of the marked difference in size between NMIIA (~250 kDa) and Srx (~12 kDa), multiple nonfunctional interactions may occur. Simultaneously, we also detected S100A4 following immunoprecipitation of Srx from the Srx OE cells, and the amount of Srx interacting with S100A4 also increased following $H_2O_2$ treatment (Figure 1C). As a control for nonspecific binding, lysates were exposed to Sepharose beads coupled to rabbit IgG. On the basis of studies described below, we determined that the upper bands in the input lanes of Figure 1C are S-glutathionylated S100A4 dimers, and it appears that the Srx immunoprecipitates primarily contain this post-translationally modified S100A4.

Immunocytochemistry showed that both S100A4 and NMIIA colocalized with Srx in the perinuclear region of A549 cells, providing additional evidence that these proteins interact in A549 cells (Figure 2; also note the strong Srx staining around the plasma membrane). These data did not distinguish whether the interaction between Srx and S100A4 is direct or indirect, i.e., as part of the complex with NMIIA. Therefore, in silico modeling and in vitro studies were performed to interrogate possible direct interactions between Srx and S100A4. Molecular modeling shows a best-fit complex between the Srx and S100A4 homodimer (Figure 1D). In this model, Srx interacts with a monomer of intact dimeric S100A4 (PDB entry 2Q91). In this complex, the proximity (~13 Å) of the single catalytic Cys99 of Srx to the conserved Cys86 of S100A4 could provide a redox-sensitive environment for the modification of either cysteine and be critical for the stability of this complex. Cys81 occurs in the same canonical target binding cleft ($\alpha$-helix) of the S100A4 monomer and may also participate in redox-dependent binding with Srx. In addition, covalent modification of Cys81 was previously shown to inhibit S100A4−NMII binding.[22] To address binding of Srx to S100A4, we studied the Srx−S100A4 interaction in vitro using FRET-based analysis of fluorescently labeled proteins. Further, to understand the role of the Srx catalytic Cys99 in its binding to S100A4, we utilized a catalytically inactive C99S mutant of Srx. Our data show reasonable binding affinity for the recombinant human (rh) S100A4 with purified intact Srx (apparent equilibrium $K_D$ ~ 83.0 nM). The affinity of rhS100A4 for the inactive Srx C99S mutant was higher (apparent equilibrium $K_D$ ~ 43.0 nM), suggesting that the catalytic cysteine of Srx is of consequence to this binding (Figure 3A). S100A1, S100A4, S100A6, and S100A9 are all substrates for S-glutathionylation in vivo.[20−22] S100A1 is closely related to S100A4, and S-glutathionylation of its Cys85 (homologous to Cys86 of S100A4) increases its $Ca^{2+}$


dx.doi.org/10.1021/bi301006w | *Biochemistry* 2012, 51, 7740−7754

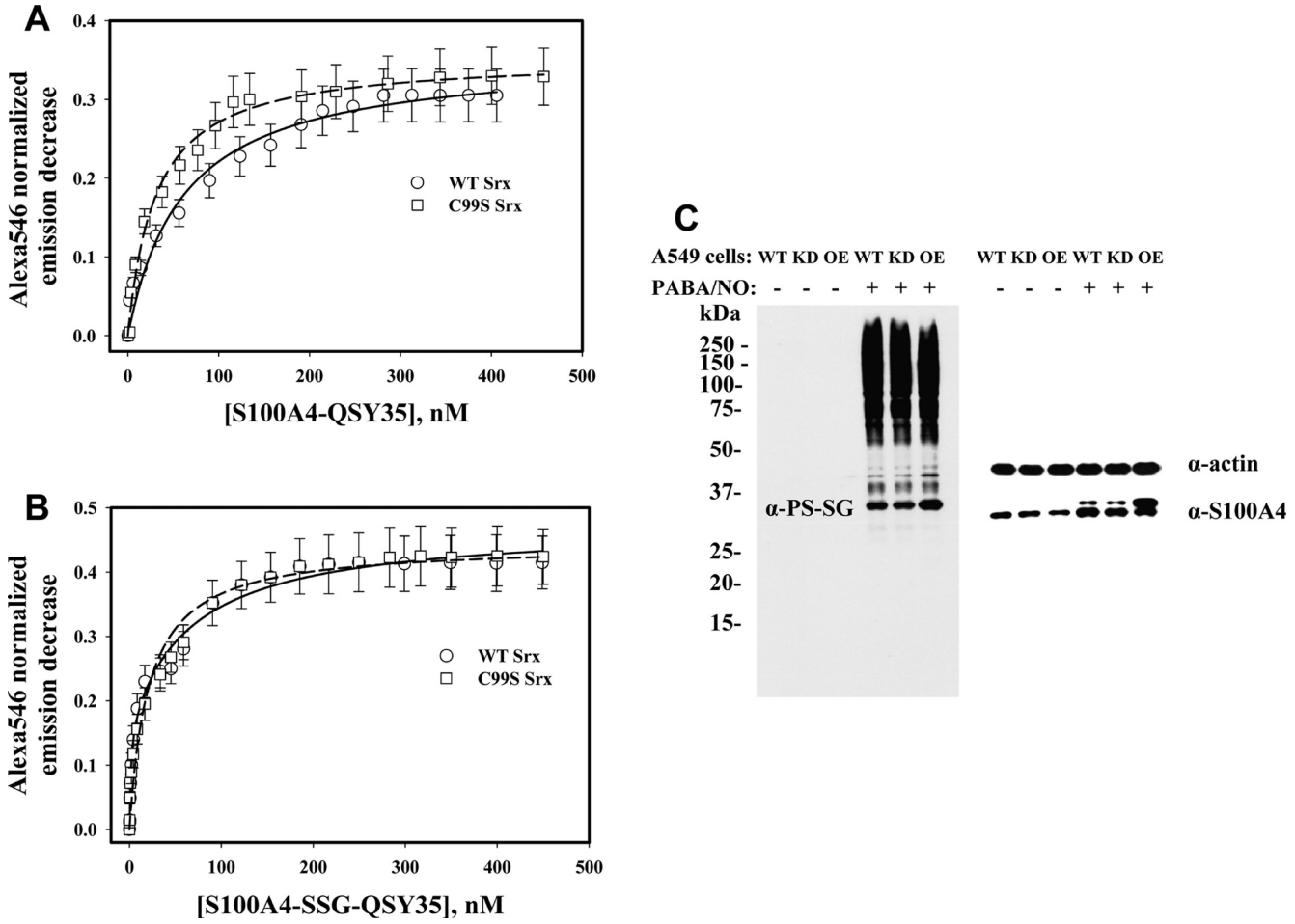


**Figure 3.** Effect of S-glutathionylation of S100A4 on its specific binding to Srx(C99S) in vitro and in A549 cells. Fluorescence analysis (for details, see Experimental Procedures) of binding of S100A4-QSY35 (A) and S100A4-SSG-QSY35 (B) to WT (C99S) Srx–Alexa546 [2.0 nM (A) and 1 nM (B)]. Solid and dashed lines represent hyperbolic fits of experimental data (for binding parameters, see Table 2). (C) Effect of Srx expression levels in A549 cells on PABA/NO-induced S-glutathionylation of S100A4. Cell lysates from untreated control cells and cells treated with 20 $\mu$M PABA/NO for 20 min were resolved by SDS–PAGE and immunoblotted with antibodies against S-glutathionylated proteins (PS-SG, left) or S100A4 on the same blot (right). Equal loading was shown by actin detection on the same blot (right). The top bands migrating at ~30 kDa on the S100A4 blot superimpose with the lowest bands on the PS-SG blot, suggesting that the S100A4 homodimer is S-glutathionylated and the increased level of Srx expression results in an increased level of S-glutathionylation of S100A4 under these conditions. The blots are representative of three independent experiments.

**Table 2. Effect of S-Glutathionylation (SSG) and $Ca^{2+}$ on Binding of S100A4 to Srx(C99S)[a]**

| | S100A4 | | S100A4-SSG | |
|---|---|---|---|---|
| Srx | EGTA | $Ca^{2+}$ | EGTA | $Ca^{2+}$ |
| WT | $K_D$ = 83.6 ± 10.6 nM | $K_D$ = 60.9 ± 8.6 nM | $K_{D1}$ = 4.9 ± 0.5 nM | $K_{D1}$ = 3.5 ± 0.6 nM |
| | | | $B_{max1}$ = 0.18 ± 0.02 | $B_{max1}$ = 0.17 ± 0.03 |
| | $B_{max}$ = 0.31 ± 0.01 | $B_{max}$ = 0.31 ± 0.01 | $K_{D2}$ = 124.5 ± 25.1 nM | $K_{D2}$ = 122.3 ± 21.3 nM |
| | | | $B_{max2}$ = 0.38 ± 0.03 | $B_{max2}$ = 0.37 ± 0.03 |
| C99S | $K_D$ = 42.9 ± 3.4 nM | $K_D$ = 30.4 ± 2.8 nM | $K_D$ = 24.0 ± 2.1 nM | $K_D$ = 21.0 ± 3.0 nM |
| | $B_{max}$ = 0.32 ± 0.01 | $B_{max}$ = 0.31 ± 0.01 | $B_{max}$ = 0.43 ± 0.02 | $B_{max}$ = 0.43 ± 0.01 |

[a]For experimental details see Experimental Procedures. Data represent means ± the standard error for three independent experiments.

binding affinity.[20] In addition, the thiol reactive drug NSC 95397 can modify Cys81 and Cys86 of S100A4, where treatment inhibits the interaction between S100A4 and NMIIA.[22] Thus, we S-glutathionylated purified rhS100A4 in vitro and studied its binding to WT Srx and the Srx C99S mutant. The affinity of S-glutathionylated S100A4 for WT Srx was markedly enhanced compared to that of intact protein, and Srx–S100A4 binding became biphasic (apparent equilibrium $K_{D1}$ = 4.8 nM and $K_{D2}$ = 131.0 nM), most likely as a consequence of a specific effect of the GSH moiety on the S100A4 surface. It is plausible that high-affinity binding of S100A4-SSG affects the structure of Srx and results in formation of low-affinity binding sites. S-Glutathionylation of S100A4 mildly affected its binding to the catalytically inactive Srx C99S mutant (apparent equilibrium $K_D$ ~ 21.0 nM), indicating a role for this residue in formation of the Srx–


dx.doi.org/10.1021/bi301006w | *Biochemistry* 2012, 51, 7740–7754

S100A4-SSG complex (Figure 3B and Table 2). Thus, the upper bands in Figure 1C likely represent S-glutathionylated S100A4 that is preferentially bound by Srx.

**Srx Influences S-Glutathionylation of S100A4.** We have previously used NO donors to induce S-glutathionylation of a variety of proteins.[28] As anticipated, treatment of A549 cells [control (WT), Srx depleted by shRNA (KD), and Srx-overexpressing (OE)] with the NO donor PABA/NO (20 $\mu$M, 20 min) increased the level of S-glutathionylation of multiple proteins in all cases (Figure 3C, left panel). The untreated control cells displayed no detectable S-glutathionylation. Reprobing the same blot with the anti-S100A4 antibody revealed that the S100A4 dimer was S-glutathionylated; the top band migrating at ~30 kDa on the S100A4 blot superimposes with the bottom band on the PS-SG blot, suggesting that the S100A4 dimer is S-glutathionylated. Further, the level of S-glutathionylation of S100A4 is markedly increased in Srx OE cells (Figure 3C, right panel). Reprobing of the same blot with the anti-actin antibody demonstrated similar protein loading in all lanes (Figure 3C, right panel). These data indicate that Srx directly influences S100A4 homeostasis in A549 cells.

Next we tested the effect of $Ca^{2+}$ on the interaction of WT Srx and Srx(C99S) with S100A4 and S-glutathionylated S100A4 (S100A4-SSG). The affinity of S100A4 for Srx was increased by $Ca^{2+}$ (Table 2). Binding of $Ca^{2+}$ to S100A4 is known to affect its conformation and promote binding to target proteins.[36] Circular dichroism (CD) showed that S-glutathionylation had a minimal impact upon S100A4 secondary structure (Figure 4A). In the presence of $Ca^{2+}$, we detected a small decrease in the $\alpha$-helical content of S-glutathionylated S100A4, likely corresponding to a slight increase in protein hydrophobicity (Figure 4A). The CD spectra of intact S100A4 with $Ca^{2+}$ almost coincide with those of S100A4-SSG with $Ca^{2+}$, so they are not presented.

Generally, protein tryptophan fluorescence can be used to evaluate tertiary and/or quaternary structural changes. However, because S100A4 does not have tryptophanyl residues, we used the tyrosine fluorescence of rhS100A4 (Figure 4B) and rhS100A4-SSG (Figure 4C) to demonstrate that $Ca^{2+}$ decreased the fluorescence (emission at ~304 nm) of S100A4, indicating conformational changes that altered the exposure of tyrosine to the polar environment. For the S-glutathionylated S100A4, $Ca^{2+}$ binding produced a pronounced change in the protein tertiary and/or quaternary structure, measured as an increase in the nonionizable, excited state for tyrosine−tyrosinate at ~345 nm.[37] These data indicate effective binding of $Ca^{2+}$ to both intact and S-glutathionylated S100A4 causing alterations in the tertiary (quaternary) structure of the latter. Accordingly, our data show that generally the affinity of Srx for S100A4 (S100A4-SSG) was increased by the presence of $Ca^{2+}$ (Table 2).

**S-Glutathionylation of S100A4 in Vitro.** HPLC analysis of the starting material and products of S100A4 S-glutathionylation by the mixture of PABA/NO and GSH in vitro was conducted to confirm that the S-glutathionylated S100A4 used in the in vitro binding studies was homogeneous. HPLC analysis showed completion of the reaction in 1.0 h at room temperature (Figure 5). The reaction mixture contained 2 nmol of S100A4, 2.5 nmol of PABA/NO, and 50.0 nmol of GSH in 1.0 mL of 10 mM PB (pH 7.4). The starting intact S100A4 was undetected in the reaction mixture after 1.0 h. After incubation for 1.0 h, PABA/NO and GSH concentrations were decreased by 62 and 80%, respectively. The retention time

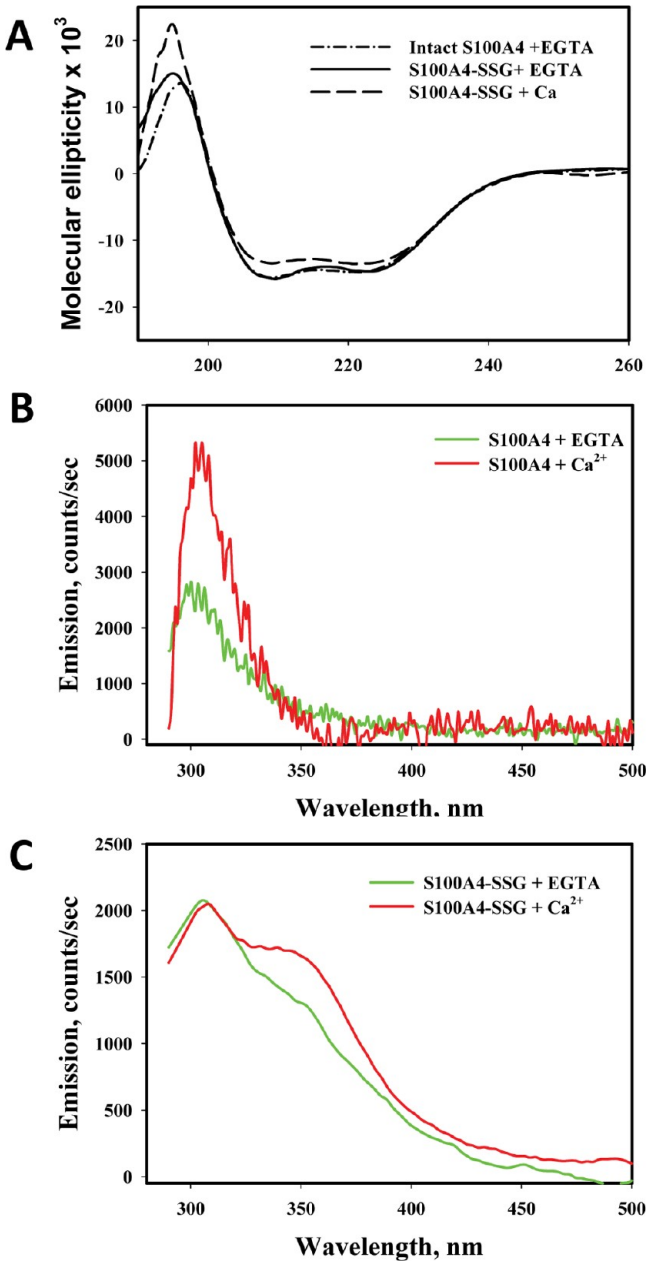


**Figure 4.** Recombinant human S100A4 (or S100A4-SSG) structure influenced by $Ca^{2+}$ and S-glutathionylation in vitro. (A) Influence of S-glutathionylation and $Ca^{2+}$ on S100A4 protein secondary structure measured by circular dichroism (note that the CD spectrum of S100A4 with $Ca^{2+}$ essentially duplicated the spectrum of S100A4-SSG with $Ca^{2+}$ and is not presented). (B and C) Effect of $Ca^{2+}$ (100 $\mu$M, red trace) or EGTA (2 mM, green trace) on tyrosine fluorescence of intact (B) or S-glutathionylated (C) rhS100A4. Traces are representative of three independent experiments.

($t_R$) for intact PABA/NO was ~5.25 min and increased after reaction for 1.0 h to ~5.35 min. $t_R$ for intact S100A4 was ~10 min and increased after incubation for 1.0 h to 10.5 min. $t_R$ for GSH (~8.65 min) was not affected by the reaction. SEC of reaction products with micro BioSpin 6 columns (Bio-Rad) resulted in isolation of >98% chromatographically homogeneous S-glutathionylated S100A4. This material, together with intact S100A4 protein, was used for titration of Srx and C99S. PABA/NO has a strong absorbance peak at ~215 nm, and its magnitude increased by ~50% after reaction for 1.0 h with


dx.doi.org/10.1021/bi301006w | Biochemistry 2012, 51, 7740−7754

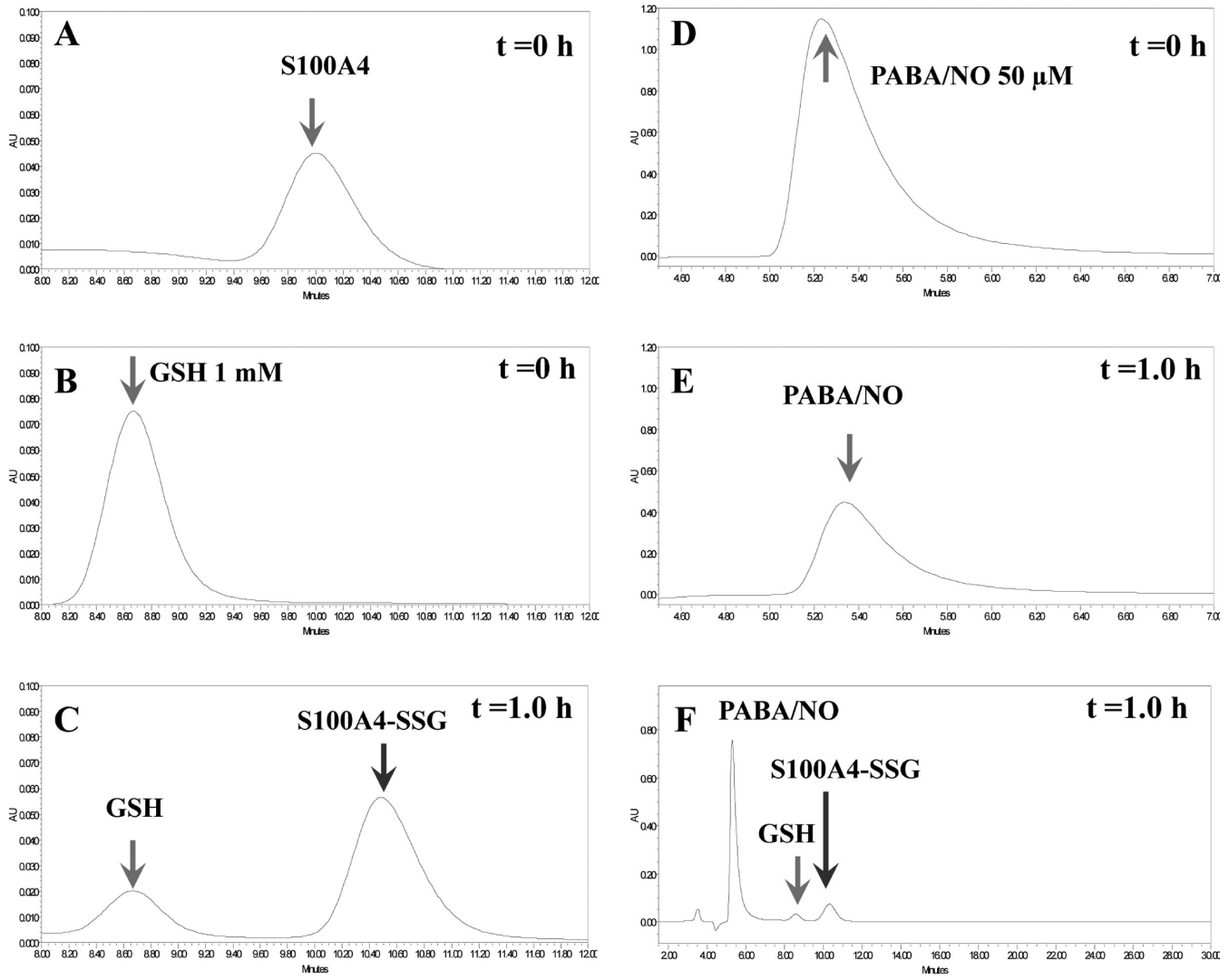


**Figure 5.** HPLC analyses of in vitro S100A4 glutathionylation by PABA/NO and GSH. Our data show completion of S100A4 S-glutathionylation [retention time ($t_R$) increases from 10.0 to 10.5 min] in 1 h at room temperature. This reaction was accompanied by a decrease in the magnitude of the GSH peak (~80%) without changes in $t_R$ (8.65 min) as well as by a decrease in the magnitude of the PABA/NO peak (~62%) with a subsequent increase in $t_R$ from 5.25 to 5.35 min.

GSH.[27] Thus, the decrease in the magnitude of the PABA/NO peak is indicative of its reaction with GSH and S100A4 protein.

Our control experiments show that the affinity of S100A4 for Srx or Srx(C99S) was essentially unaffected by labeling of the latter with Alexa546. The apparent equilibrium dissociation constants for labeled Srx ($K_D$ ~ 61 nM) or Srx(C99S) ($K_D$ ~ 30 nM) were similar to those for mixtures to which unlabeled intact Srx ($K_D$ ~ 60 nM) or Srx(C99S) ($K_D$ ~ 28 nM) had been added (all competition experiments were performed with standard additions of $Ca^{2+}$). In comparison, the number of binding complexes for labeled Srx or Srx(C99S) ($B_{max}$ ~ 0.31 or 0.31, respectively) were essentially halved in the presence of unlabeled, intact Srx or Srx(C99S) [$B_{max}$ ~ 0.13 or 0.15, respectively (Figure 6A,B)]. Additionally, we show that labeling of S100A4 with QSY35 does not substantially affect its binding to Srx(C99S). The back-titration of Alexa546-labeled Srx(C99S), preincubated with 150 nM QSY35-labeled S100A4, with unlabeled intact S100A4 almost halved its level of binding (Figure 6C). Intrinsic equilibrium dissociation constants calculated from back-titrations of labeled Srx or Srx(C99S) with intact S100A4 ($K_D$ ~ 63.0 or 33.0 nM, respectively) were similar to those for QSY35-labeled S100A4 (Table 2, experiments performed with standard additions of $Ca^{2+}$). While increased displacement of labeled S100A4 binding to Srx(C99S) by higher concentrations of intact protein infers some differences in binding between WT and mutant Srx (Figure 6C), our data confirmed that the effects of fluorescence labeling on Srx(C99S)−S100A4 binding were minimal.

**Srx Levels Influence Filamentous Actin Structures and Cell Adhesion.** We examined the impact of Srx expression levels on actin cytoskeletal structure and function. A549 cells with Srx expression levels at normal (WT), depleted by shRNA (Srx KD), or overexpressing (Srx OE) were used to visualize the effect of Srx on filamentous actin and $Tyr^{397}$-phosphorylated focal adhesion kinase (P-FAK). Immunofluorescent staining of A549 cells showed that Srx influenced both cytoskeletal architecture and focal contacts (Figure 7). For example, Srx OE cells exhibited more prominent stress fibers and more mature, but less numerous, focal adhesions. By contrast, control and Srx KD cells had reticular patterns of microfilaments. Srx KD cells also had more numerous but less mature focal contacts compared to both control and Srx OE


dx.doi.org/10.1021/bi301006w | *Biochemistry* 2012, 51, 7740−7754

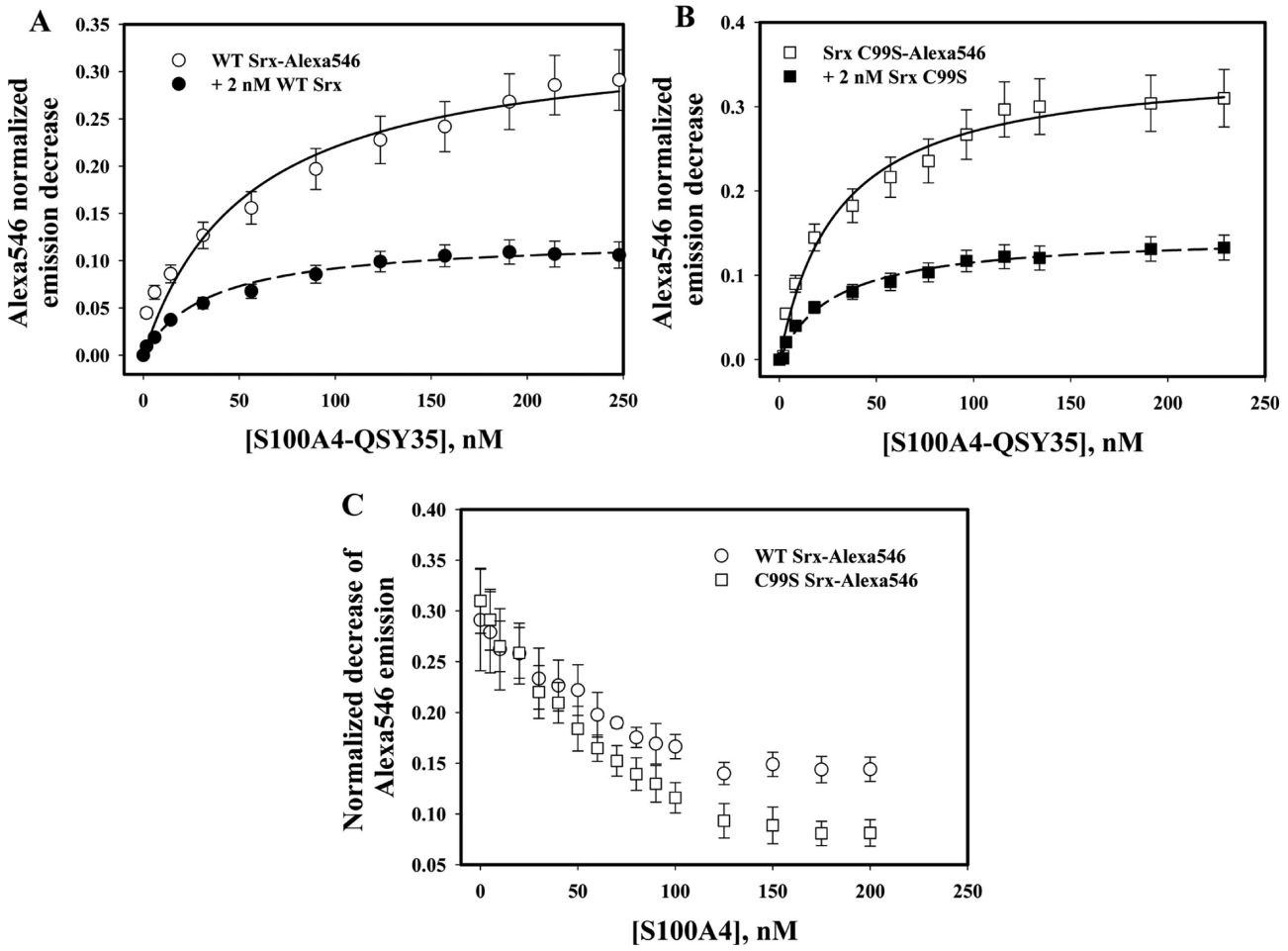


**Figure 6.** Effect of Srx(C99S) and S100A4 fluorescence labeling on their binding affinity. Addition of unlabeled intact Srx(C99S) proteins (both at 2.0 nM) to Alexa546-labeled Srx (A) or C99S (B) (both at 2.0 nM) results in an ~2-fold decrease in the number of binding sites for S100A4-QSY35 without significantly altering binding affinities. Binding isotherms representing back-titrations of Srx− or Srx(C99S)−Alexa546 (both at 2.0 nM, preincubated with 150 nM S100A4-QSY35) with unlabeled intact S100A4 result in competitive proportional displacement of labeled S100A4 (C). Data are means ± SD for three independent experiments. In panels A and B, solid (WT Srx) and dashed [Srx(C99S)] lines represent hyperbolic fits ($R^2$ = 0.99) of experimental data (see Experimental Procedures for details).

cells. Further, P-FAK staining of Srx KD cells was less prominent on the periphery of the cells and more prominent in the perinuclear region compared to both control and Srx OE cells.

For further investigation of the role of Srx in cell adhesion and microfilament structure, we performed adhesion assays and measured the ratio of globular to filamentous actin in cells with variable Srx levels. Confirmation that shRNA depleted Srx (essentially below detection) and that transfection increased Srx (~4-fold) levels is shown in Figure 8A. More Srx KD cells adhered to fibronectin-coated dishes than control cells, whereas significantly fewer Srx OE cells adhered (Figure 8B). Commensurate with adhesion, compared to WT cells, Srx KD cells had an increased ratio of P-FAK to total FAK and Srx OE cells had a decreased ratio, although this trend did not reach statistical significance (Figure 8C). In addition, Srx OE cells had an increased ratio of globular (G) to filamentous (F) actin compared to both control and Srx KD cells (Figure 8D). Although the decreased level of adhesion and filamentous actin in Srx OE cells might appear to contradict the immunofluoresence data where actin stress fibers and focal adhesions are clearly visible in Srx OE cells, it should be noted that the immunoblots of P-FAK and G and F actin permit quantification of total cellular levels of these proteins. Immunofluoresence shows large, mature focal adhesions of Srx OE cells apparently outnumbered by nascent adhesions and less mature focal contacts in the control and Srx KD cells (Figure 7). Similarly, although Srx OE cells display prominent stress fibers that are bundles of F actin, the control and Srx KD cells have more F actin. Overall, these data show that Srx has a marked effect on the cytoskeletal architecture and adhesion of A549 cells.

**Srx Levels Affect Cell Motility.** We hypothesized that the Srx−S100A4−NMIIA interaction should influence cell migration. To test this, we performed scratch assays using A549 cells with varying degrees of Srx expression. Srx overexpression resulted in a substantial increase in the rate of gap filling between "wound" edges, implying enhanced planar cell motility (Figure 9). In addition, migration by Srx knockdown cells was significantly slower than in cells with WT Srx levels. For these experiments, we used two independent overexpressing or knockdown and vector only control cell lines (WT Srx), and all gave consistent results that Srx expression influences the motility of A549 cells.


dx.doi.org/10.1021/bi301006w | *Biochemistry* 2012, 51, 7740−7754

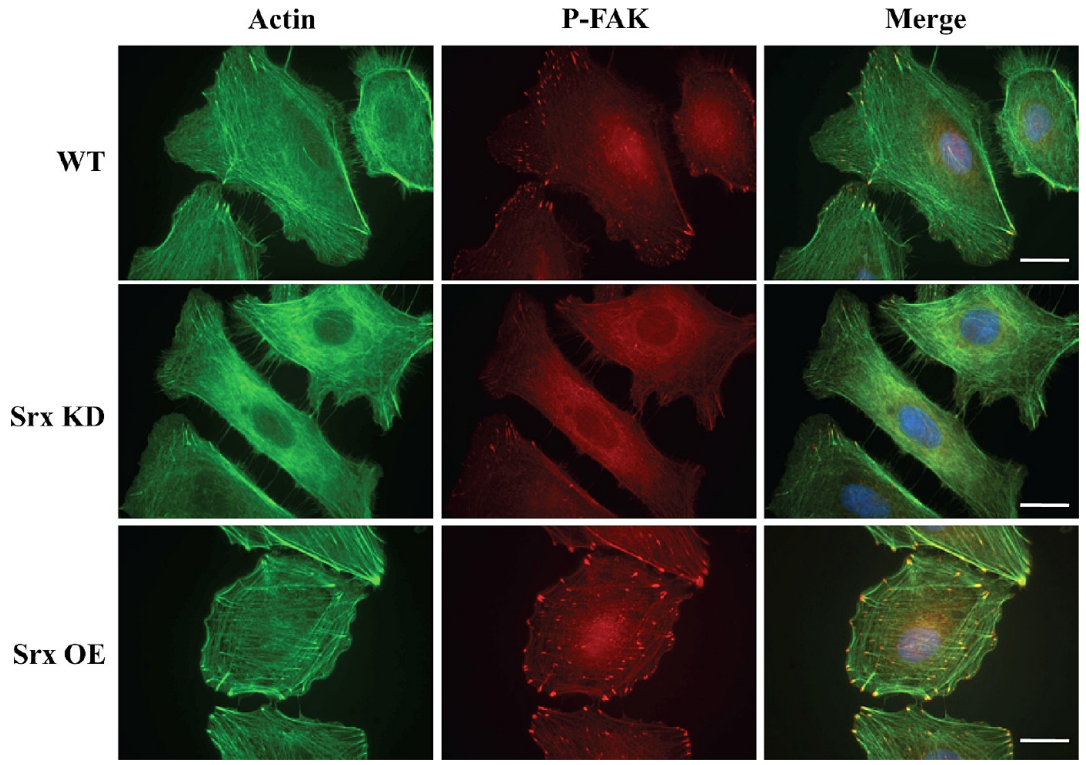


**Figure 7.** Sulfiredoxin expression levels affect filamentous actin and focal contacts in A549 cells. A549 cells with control Srx levels (WT Srx), Srx knockdown (Srx KD), or Srx overexpression (Srx OE) were seeded onto fibronectin-coated glass chamber slides, and after 24 h, cells that had not adhered were removed and filamentous actin and focal adhesions visualized by flourescently abeled phalloidin and immunocytochemistry of $Tyr^{397}$-phosphorylated-FAK. The bar represents 10 $\mu$m.

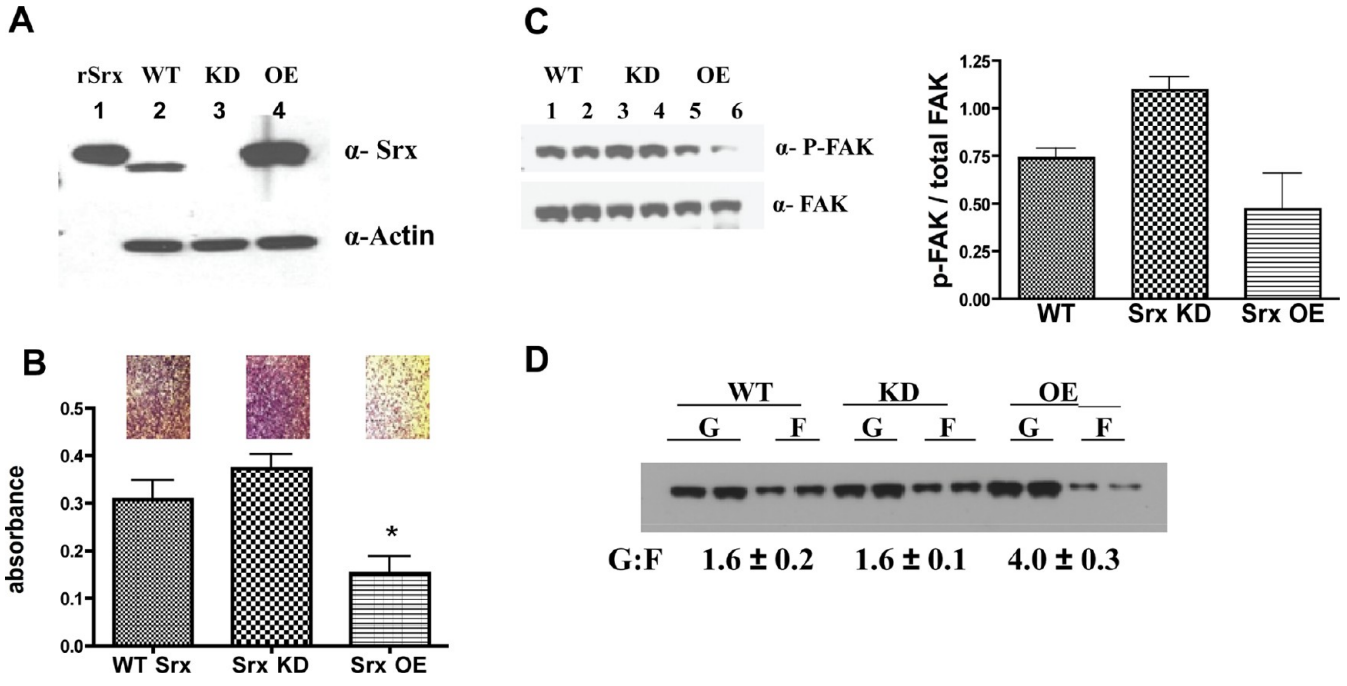


**Figure 8.** Sulfiredoxin affects adhesion of A549 cells to fibronectin, phospho-focal adhesion kinase, and filamentous actin levels in A549 cells. (A) Immunoblot of the cells used in panels B–D: lane 1, recombinant Srx; lane 2, A549 whole cell extract with WT Srx levels; lane 3, Srx KD; lane 4, Srx OE cells. Where relevant, the actin loading control is shown below. (B) A549 cells [control (WT), shRNA-depleted (Srx KD), or Srx-overexpressing (Srx OE)] were plated on dishes coated with fibronectin, and the number of cells that adhered after 2 h was quantified as described in Experimental Procedures. The insets are photomicrographs of crystal violet-stained A549 cells in adhesion assays. (C) Immunoblots of $Tyr^{397}$-phosphorylated FAK and total FAK in A549 cells with variable levels of Srx expression after adhesion to fibronectin for 24 h. (D) A549 cells as in panel A were seeded onto fibronectin-coated cell culture dishes, and after 24 h, cells were lysed and the ratio of globular (G) to filamentous (F) actin was quantified. The data shown are representative of three independent experiments.


dx.doi.org/10.1021/bi301006w | *Biochemistry* 2012, 51, 7740–7754

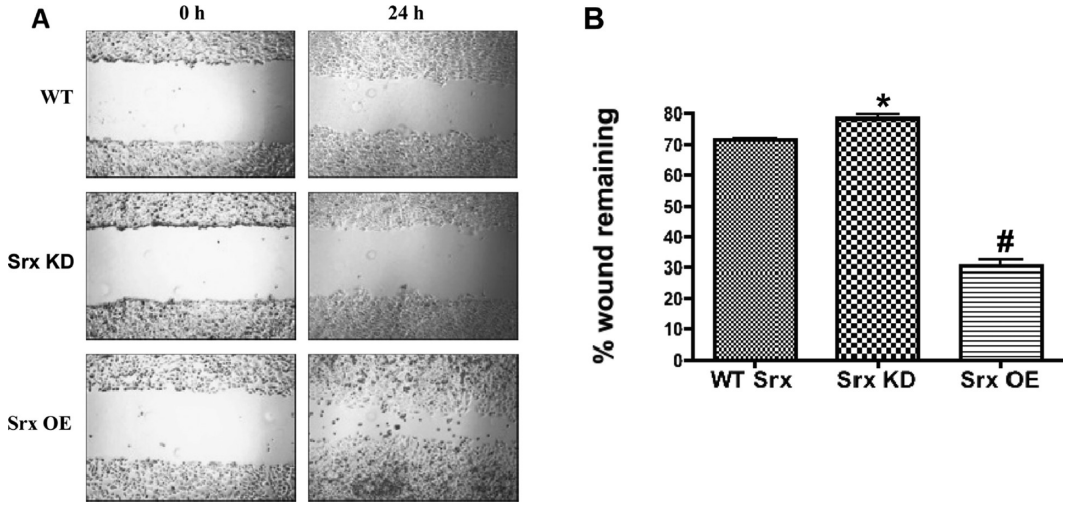


**Figure 9.** Overexpression of sulfiredoxin in A549 cells results in an increased level of cell migration as determined by a scratch assay. (A) Wild-type A549 cells, A549 cells with Srx depleted by shRNA (Srx KD), and A549 cells overexpressing Srx (Srx OE) were plated in 3.5 cm dishes and allowed to reach confluence. Cell monolayers were "wounded" with a pipet tip and photomicrographs acquired immediately afterward and at 24 h. (B) Quantification of three independent experiments as shown in panel A using ImageJ. Bars with different symbols are significantly different ($P < 0.05$, ANOVA) from each other.

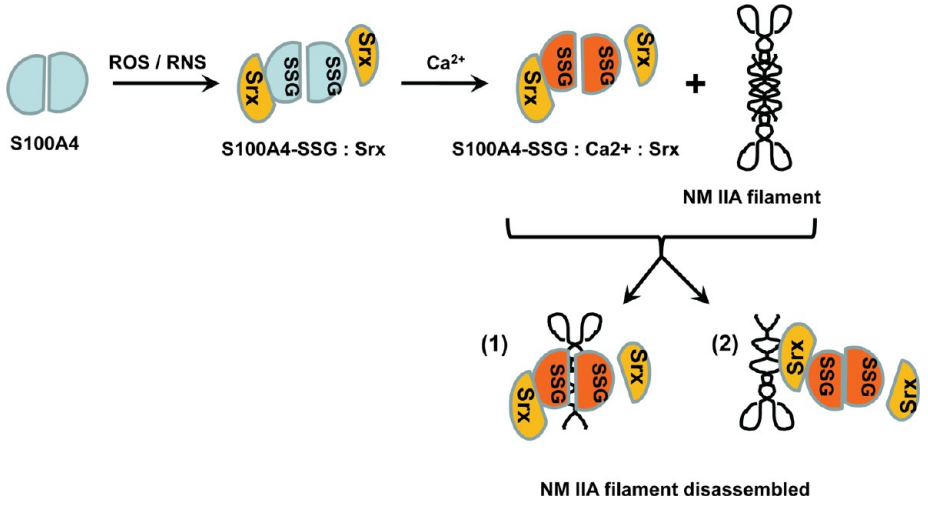


**Figure 10.** Model of the effect of redox specific Srx–S100A4–NMII interactions on the motility and mobility of A549 cells. S100A4 (light blue hemispheres) under oxidative (ROS) or nitrosative (RNS) stress conditions undergo S-glutathionylation and subsequent loading with $Ca^{2+}$. Srx (yellow hemispheres) binds to the S-glutathionylated and $Ca^{2+}$-loaded S100A4 (orange hemispheres), forming a heterotetramer structure. This Srx–S100A4 complex then targets NMIIA filaments either (1) through S100A4 or (2) through Srx, in either case promoting NMIIA filament disassembly and consequently promoting cell migration.

## DISCUSSION

This study identifies S100A4 and NMIIA as novel Srx binding partners. Within this context, Srx influences cell migration, adhesion, and cytoskeletal architecture. Srx forms a complex with S100A4, the stability of which is enhanced by S-glutathionylation of the latter. We propose that S-glutathionylation of S100A4 increases its affinity for $Ca^{2+}$ analogous to results reported for S100A1.[20] Although Srx is reported to deglutathionylate actin, PTP1B, and PrxI,[5,8,9] in this study increased Srx levels were associated with increased levels of S100A4 S-glutathionylation while decreased Srx levels were associated with decreased levels of S100A4 S-glutathionylation. Therefore, we speculate that Srx binds to S-glutathionylated S100A4 but does not catalyze the deglutathionylation of this protein. Thus, we propose that Srx modulates S100A4 activity through an increase in the level of $Ca^{2+}$ binding and changes in specific targeting regarding NMIIA depolymerization (Figure 10). Cysteine 81 and cysteine 86 of S100A4 are implicated in S100A4–NMIIA interactions,[25] raising the possibility of redox-mediated S100A4–NMIIA interactions that may be regulated by Srx. Our proposed model of Srx promotion of S100A4–NMIIA interaction is consistent with our observations that increased levels of Srx expression leads to increased levels of cell migration. The NMIIA heavy chain can be S-nitrosylated at Cys90, -895, and -916, and in the presence of millimolar GSH, S-nitrosylated cysteines are rapidly converted to S-glutathionylated residues.[38] NMIIA may be a substrate for Srx-mediated deglutathionylation of Cys895 or -916 and would be expected to affect monomer–dimer–multimer equilibria because these residues are located in the NMIIA heavy chain dimerization domain. Thus, given that the strength of Srx and NMIIA interactions increased following oxidative stress, Srx could


dx.doi.org/10.1021/bi301006w | *Biochemistry* 2012, 51, 7740–7754

promote NMIIA activity by enacting deglutathionylation, although this possibility is not explicitly shown in the model proposed in Figure 10. This may also explain the increased level of migration of Srx OE cells in wound healing assays.

Nodal linkages between redox and various aspects of cell motility, including invasion and metastasis, have been reported. For example, a role for reactive oxygen species (ROS) generated by the NADPH oxidase (Nox) has been implicated in the formation and function of cancer cell invadopodia. Specifically, Tks5 facilitates the production of ROS, determined to be necessary for the formation of invadopodia, and in turn, ROS modulates Tks5 tyrosine phosphorylation in a positive feedback loop.[39] Nox family enzymes have been linked with functional aspects of invasion and metastasis,[13,14] and enhanced generation of superoxide anion radicals by Nox may result in its spontaneous dismutation into $H_2O_2$ or facilitate interaction with NO [with subsequent peroxynitrite ($NOOO^-$) generation]. Subsequent cysteine nitrosylation and/or S-glutathionylation can influence actin−myosin interactions.[16,17,40] The redox functions of Srx could contribute in providing homeostatic balance to the oxidative properties of the Nox system with consequent influence on cell motility and migration. High-level expression of Srx was shown in human solid tumors, particularly skin and lung cancers, and it was found to be required for the growth, migration, and invasion of human lung cancer cells in vitro.[2] One downstream target of Srx-mediated cell signaling is PrxIV, and knockdown of PrxIV mimicked the phenotypic changes of depleting Srx. Knockdown of Srx reduced the level of anchorage-independent growth in soft agar, the level of cell migration in a wound healing assay, and cell invasiveness.[41] Collectively, these data suggest that the Srx−PrxIV axis is critical in human lung cancer cell maintenance, migration, and invasion. Although the data presented here suggest a discrepancy in that an elevated level of Srx is linked with a reduced level of adhesion, these general conclusions are also consistent with our findings that Srx mediates these events through a multiprotein complex that could include NMIIA and S100A4.

Unexpectedly, Srx shares a quite high degree of sequence homology with members of the IQGAP family of scaffolding proteins that bind to the Rho GTPases Cdc42 and Rac1.[42] BLAST [Basic Local Alignment Search Tool (http://blast.ncbi.nlm.nih.gov)] analysis revealed that the entire coding sequence of hSrx1 is 86% identical with a region of ras GTPase-activating like protein IQGAP2. At the amino acid level, an 18-residue (18−35) region of Srx has a 50% positive relationship within a region of IQGAP2 that binds Cdc42 and Rac GTPases, suggesting possible functional similarities. Because the published crystal structure of Srx starts at amino acid residue 32 (PDB entry 1XW3), the structural model of Srx shown in Figure 2B excludes 14 of 18 residues from the homologous site, and the four residues that are shown are not structured. Attempts to crystallize full-length Srx have been unsuccessful, reportedly because of the glycine-rich nature of the N-terminal region of Srx. Under physiological conditions, it is conceivable that the region of Srx with homology to IQGAP2 could form a structure that allows Cdc42−Rac GTPase binding. Moreover, because the members of the IQGAP family are integral to many aspects of cytoskeletal regulation[42] and tumorigenesis,[43] this structural overlap with Srx may indicate some divergent evolutionary relationship worthy of further consideration.

Actin−NMIIA interactions in non-muscle cells are mediated by fully $Ca^{2+}$-loaded S100A4, and our results show that binding of $Ca^{2+}$ by S100A4 is influenced by its S-glutathionylation. S-Glutathionylation of Cys85 of S100A1 also causes structural modifications and enhanced $Ca^{2+}$ binding.[20] The most conserved regions within the S100 protein family are the $Ca^{2+}$-binding motifs, the EF-hands, which are involved in subunit dimerization conferring biological functionality.[44] $Ca^{2+}$-loaded S100A4 binds to NMIIA via a motif at the C-terminal end of the coiled-coil region of myosin, and the interaction results in the disassembly of myosin filaments.[23] Its tight affinity for $Ca^{2+}$ is increased by several orders of magnitude in the presence of NMIIA. By binding to the C-terminal EF-hand of S100A4, $Ca^{2+}$ causes a large conformational change and exposes a hydrophobic surface containing residues in the hinge region, $\alpha$-helices III and IV, and the C-terminal loop. This hydrophobic surface is part of the NMIIA recognition site stabilizing the quaternary structure of the complex.[23] This is consistent with our data [increased emission of deprotonated tyrosine (tyrosinate)[37]] indicating that the tertiary and quaternary structures of S100A4 (and in particular S100A4-SSG) are influenced by $Ca^{2+}$ (Figure 4C). Tyr75 ($\alpha$-helix IV) of S100A4 is essential for homodimerization.[45] Specific to S100A4, the proximity of Cys76 to Tyr75 could be relevant to our tyrosinate fluorescence data that indicate tertiary and quaternary structural changes. Thus, Cys76 S-glutathionylation may shift the S100A4 monomer−dimer equilibrium. Our present in vitro data support such a hypothesis, but further experiments will be required to prove that this occurs in vivo. Because of its tight binding to S-glutathionylated S100A4, increased levels of Srx may promote S100A4 activity toward NMIIA. Our titration data (using 0−0.5 $\mu$M S100A4 and S100A4-SSG) showed that binding to Srx and SrxC99S is specific and is enhanced by $Ca^{2+}$ (Table 2), regardless of the fact that the interface of these proteins [amino acids 51−64 ($\alpha$-helix III) for S100A4 and amino acids 130−136 for Srx] does not involve the EF-hand motifs [molecular modeling (Figure 1D)]. An increase in the affinity of S-glutathionylated S100A4 for Srx signifies an increased stability of this complex and, consequently, may result in Srx specific targeting of NMII. The latter could affect the bound or free state of the S100A4−Srx complex and $Ca^{2+}$ equilibrium for the actin−NMII interaction. Our data suggest that low-affinity binding of Srx with S-glutathionylated S100A4 might occur only after saturation of the high-affinity binding sites. Such high-affinity binding may cause structural changes only in Srx (not Srx C99S), implying that the Cys99 in Srx is involved in heterodimerization with S100A4.

The "floodgate" hypothesis of $H_2O_2$ signaling considers that peroxiredoxins are inactivated by hyperoxidation to allow local accumulation of $H_2O_2$ for signaling purposes.[46] Thus, Srx can reactivate peroxiredoxins maintaining "physiological" $H_2O_2$ levels. However, hyperoxidized peroxiredoxins cannot be detected during physiological $H_2O_2$ signaling,[47] and phosphorylation of Tyr194 of membrane-associated PrxI inactivates it following growth factor stimulation during wound healing, allowing a transient accumulation of $H_2O_2$ around membranes.[48] This implies that in addition to reducing overoxidized peroxiredoxins there may be further physiological functions for Srx. Our results define a role for Srx as a redox-regulated specific S100A4 carrier, participating in cytoskeleton remodeling functioning in cellular mobility and motility regulation. Overall, we propose the model in Figure 10, which is consistent with the data generated. Initial S-glutathionylation of S100A4 mechanistically activates it through increasing its binding affinity for $Ca^{2+}$, thereby exposing internal hydrophobic areas

of the monomers. Srx binds with high affinity to the S-glutathionylated and $Ca^{2+}$-loaded S100A4, stabilizing the active S100A4. Srx bound to S100A4 then binds to NMIIA through either (i) S100A4−NMIIA binding or (ii) Srx−NMIIA binding, in either case promoting NMIIA filament disassembly and thereby affecting cell migration and adhesion. This model supports the conclusion that interactions of Srx with NMIIA and S100A4 have a functional redox role in controlling cell motility, migration, and adhesion.

## AUTHOR INFORMATION


### Corresponding Author

*Department of Cell and Molecular Pharmacology and Experimental Therapeutics, Medical University of South Carolina, Charleston, SC 29425. Phone: (843) 792-2514. Fax: (843) 792-9588. E-mail: tewk@musc.edu.



### Funding

This work was supported by grants from the National Institutes of Health (CA08660 and CA117259), the National Center for Research Resources (5P20RR024485-02), and the National Institute of General Medical Sciences (8 P20 GM103542-02) and the South Carolina Centers of Excellence program.


### Notes

The authors declare no competing financial interests.

## ACKNOWLEDGMENTS


We thank the Drug Metabolism and Pharmacokinetics and Proteomics Core Facilities at the Medical University of South Carolina. This work was conducted in a facility constructed with support from the National Institutes of Health (Grant C06 RR015455) from the Extramural Research Facilities Program of the National Center for Research Resources.


## ABBREVIATIONS

FAK, focal adhesion kinase; GSH, glutathione; KD, knockdown; NMIIA, nonmuscle myosin IIA; NOS, nitric oxide synthase; NOX, NADPH oxidase; OE, overexpressing; PABA/NO, $O^2$-{2,4-dinitro-5-[4-(*N*-methylamino)benzoyloxy]-phenyl}-1-(*N*,*N*-dimethylamino)diazen-1-ium-1,2-diolate; Prx, peroxiredoxin; Srx, sulfiredoxin.

## REFERENCES


(1) Finkel, T. (2011) Signal transduction by reactive oxygen species. *J. Cell Biol. 194*, 7−15.

(2) Wei, Q., Jiang, H., Matthews, C. P., and Colburn, N. H. (2008) Sulfiredoxin is an AP-1 target gene that is required for transformation and shows elevated expression in human skin malignancies. *Proc. Natl. Acad. Sci. U.S.A. 105*, 19738−19743.

(3) Planson, A. G., Palais, G., Abbas, K., Gerard, M., Couvelard, L., Delaunay, A., Baulande, S., Drapier, J. C., and Toledano, M. B. (2011) Sulfiredoxin Protects Mice from Lipopolysaccharide-Induced Endotoxic Shock. *Antioxid. Redox Signaling 14*, 2071−2080.

(4) Bae, S. H., Sung, S. H., Cho, E. J., Lee, S. K., Lee, H. E., Woo, H. A., Yu, D. Y., Kil, I. S., and Rhee, S. G. (2011) Concerted action of sulfiredoxin and peroxiredoxin I protects against alcohol-induced oxidative injury in mouse liver. *Hepatology 53*, 945−953.

(5) Park, J. W., Mieyal, J. J., Rhee, S. G., and Chock, P. B. (2009) Deglutathionylation of 2-Cys peroxiredoxin is specifically catalyzed by sulfiredoxin. *J. Biol. Chem. 284*, 23364−23374.

(6) Woo, H. A., Jeong, W., Chang, T. S., Park, K. J., Park, S. J., Yang, J. S., and Rhee, S. G. (2005) Reduction of cysteine sulfinic acid by sulfiredoxin is specific to 2-cys peroxiredoxins. *J. Biol. Chem. 280*, 3125−3128.

(7) Biteau, B., Labarre, J., and Toledano, M. B. (2003) ATP-dependent reduction of cysteine-sulphinic acid by *S. cerevisiae* sulphiredoxin. *Nature 425*, 980−984.

(8) Findlay, V. J., Townsend, D. M., Morris, T. E., Fraser, J. P., He, L., and Tew, K. D. (2006) A novel role for human sulfiredoxin in the reversal of glutathionylation. *Cancer Res. 66*, 6800−6806.

(9) Lei, K., Townsend, D. M., and Tew, K. D. (2008) Protein cysteine sulfinic acid reductase (sulfiredoxin) as a regulator of cell proliferation and drug response. *Oncogene 27*, 4877−4887.

(10) Vicente-Manzanares, M., Ma, X., Adelstein, R. S., and Horwitz, A. R. (2009) Non-muscle myosin II takes centre stage in cell adhesion and migration. *Nat. Rev. Mol. Cell Biol. 10*, 778−790.

(11) Garrett, S. C., Varney, K. M., Weber, D. J., and Bresnick, A. R. (2006) S100A4, a mediator of metastasis. *J. Biol. Chem. 281*, 677−680.

(12) Parsons, J. T., Horwitz, A. R., and Schwartz, M. A. (2010) Cell adhesion: Integrating cytoskeletal dynamics and cellular tension. *Nat. Rev. Mol. Cell Biol. 11*, 633−643.

(13) Kumar, B., Koul, S., Khandrika, L., Meacham, R. B., and Koul, H. K. (2008) Oxidative stress is inherent in prostate cancer cells and is required for aggressive phenotype. *Cancer Res. 68*, 1777−1785.

(14) Weaver, A. M. (2009) Regulation of cancer invasion by reactive oxygen species and Tks family scaffold proteins. *Sci. Signaling 2*, pe56.

(15) Dalle-Donne, I., Giustarini, D., Rossi, R., Colombo, R., and Milzani, A. (2003) Reversible S-glutathionylation of Cys 374 regulates actin filament formation by inducing structural changes in the actin molecule. *Free Radical Biol. Med. 34*, 23−32.

(16) Pastore, A., Tozzi, G., Gaeta, L. M., Bertini, E., Serafini, V., Di Cesare, S., Bonetto, V., Casoni, F., Carrozzo, R., Federici, G., and Piemonte, F. (2003) Actin glutathionylation increases in fibroblasts of patients with Friedreich's ataxia: A potential role in the pathogenesis of the disease. *J. Biol. Chem. 278*, 42588−42595.

(17) Wang, J., Boja, E. S., Tan, W., Tekle, E., Fales, H. M., English, S., Mieyal, J. J., and Chock, P. B. (2001) Reversible glutathionylation regulates actin polymerization in A431 cells. *J. Biol. Chem. 276*, 47763−47766.

(18) Tarabykina, S., Griffiths, T. R., Tulchinsky, E., Mellon, J. K., Bronstein, I. B., and Kriajevska, M. (2007) Metastasis-associated protein S100A4: Spotlight on its role in cell migration. *Curr. Cancer Drug Targets 7*, 217−228.

(19) Santamaria-Kisiel, L., Rintala-Dempsey, A. C., and Shaw, G. S. (2006) Calcium-dependent and -independent interactions of the S100 protein family. *Biochem. J. 396*, 201−214.

(20) Goch, G., Vdovenko, S., Kozlowska, H., and Bierzynski, A. (2005) Affinity of S100A1 protein for calcium increases dramatically upon glutathionylation. *FEBS J. 272*, 2557−2565.

(21) Lim, S. Y., Raftery, M. J., Goyette, J., and Geczy, C. L. (2010) S-Glutathionylation regulates inflammatory activities of S100A9. *J. Biol. Chem. 285*, 14377−14388.

(22) Orre, L. M., Pernemalm, M., Lengqvist, J., Lewensohn, R., and Lehtio, J. (2007) Up-regulation, modification, and translocation of S100A6 induced by exposure to ionizing radiation revealed by proteomics profiling. *Mol. Cell. Proteomics 6*, 2122−2131.

(23) Badyal, S. K., Basran, J., Bhanji, N., Kim, J. H., Chavda, A. P., Jung, H. S., Craig, R., Elliott, P. R., Irvine, A. F., Barsukov, I. L., Kriajevska, M., and Bagshaw, C. R. (2011) Mechanism of the $Ca^{2+}$-dependent interaction between S100A4 and tail fragments of nonmuscle myosin heavy chain IIA. *J. Mol. Biol. 405*, 1004−1026.

(24) Li, Z. H., and Bresnick, A. R. (2006) The S100A4 metastasis factor regulates cellular motility via a direct interaction with myosin-IIA. *Cancer Res. 66*, 5173−5180.

(25) Dulyaninova, N. G., Hite, K. M., Zencheck, W. D., Scudiero, D. A., Almo, S. C., Shoemaker, R. H., and Bresnick, A. R. (2011) Cysteine 81 is critical for the interaction of S100A4 and myosin-IIA. *Biochemistry 50*, 7218−7227.

(26) Saavedra, J. E., Srinivasan, A., Buzard, G. S., Davies, K. M., Waterhouse, D. J., Inami, K., Wilde, T. C., Citro, M. L., Cuellar, M., Deschamps, J. R., Parrish, D., Shami, P. J., Findlay, V. J., Townsend, D. M., Tew, K. D., Singh, S., Jia, L., Ji, X., and Keefer, L. K. (2006) PABA/NO as an anticancer lead: Analogue synthesis, structure revision,

solution chemistry, reactivity toward glutathione, and in vitro activity. *J. Med. Chem. 49*, 1157−1164.
(27) Manevich, Y., Townsend, D. M., Hutchens, S., and Tew, K. D. (2010) Diazeniumdiolate mediated nitrosative stress alters nitric oxide homeostasis through intracellular calcium and S-glutathionylation of nitric oxide synthetase. *PLoS One 5*, e14151.
(28) Townsend, D. M., Manevich, Y., He, L., Xiong, Y., Bowers, R. R., Jr., Hutchens, S., and Tew, K. D. (2009) Nitrosative stress-induced S-glutathionylation of protein disulfide isomerase leads to activation of the unfolded protein response. *Cancer Res. 69*, 7626−7634.
(29) Roussel, X., Bechade, G., Kriznik, A., Van Dorsselaer, A., Sanglier-Cianferani, S., Branlant, G., and Rahuel-Clermont, S. (2008) Evidence for the formation of a covalent thiosulfinate intermediate with peroxiredoxin in the catalytic mechanism of sulfiredoxin. *J. Biol. Chem. 283*, 22371−22382.
(30) Turner, J., Anderson, R., Guo, J., Beraud, C., Fletterick, R., and Sakowicz, R. (2001) Crystal structure of the mitotic spindle kinesin Eg5 reveals a novel conformation of the neck-linker. *J. Biol. Chem. 276*, 25496−25502.
(31) Saijo, T., Ishii, G., Ochiai, A., Yoh, K., Goto, K., Nagai, K., Kato, H., Nishiwaki, Y., and Saijo, N. (2006) Eg5 expression is closely correlated with the response of advanced non-small cell lung cancer to antimitotic agents combined with platinum chemotherapy. *Lung Cancer 54*, 217−225.
(32) Dorner, C., Ciossek, T., Muller, S., Moller, P. H., Ullrich, A., and Lammers, R. (1998) Characterization of KIF1C, a new kinesin-like protein involved in vesicle transport from the Golgi apparatus to the endoplasmic reticulum. *J. Biol. Chem. 273*, 20267−20275.
(33) Marsit, C. J., Okpukpara, C., Danaee, H., and Kelsey, K. T. (2005) Epigenetic silencing of the PRSS3 putative tumor suppressor gene in non-small cell lung cancer. *Mol. Carcinog. 44*, 146−150.
(34) Tyagi, S. C. (1996) Role of oxidative mixed-disulfide formation in elastase-serine proteinase inhibitor (serpin) complex. *Biochem. Cell Biol. 74*, 391−401.
(35) Durussel, I., Blouquit, Y., Middendorp, S., Craescu, C. T., and Cox, J. A. (2000) Cation- and peptide-binding properties of human centrin 2. *FEBS Lett. 472*, 208−212.
(36) Garrett, S. C., Varney, K. M., Weber, D. J., and Bresnick, A. R. (2006) S100A4, a mediator of metastasis. *J. Biol. Chem. 281*, 677−680.
(37) Lacowick, J. R. (1999) in *Principles of Fluorescence Spectroscopy*, pp 450−452, Kluwer Academic/Plenum Publishers, New York.
(38) Greco, T. M., Hodara, R., Parastatidis, I., Heijnen, H. F., Dennehy, M. K., Liebler, D. C., and Ischiropoulos, H. (2006) Identification of S-nitrosylation motifs by site-specific mapping of the S-nitrosocysteine proteome in human vascular smooth muscle cells. *Proc. Natl. Acad. Sci. U.S.A. 103*, 7420−7425.
(39) Diaz, B., Shani, G., Pass, I., Anderson, D., Quintavalle, M., and Courtneidge, S. A. (2009) Tks5-dependent, nox-mediated generation of reactive oxygen species is necessary for invadopodia formation. *Sci. Signaling 2*, ra53.
(40) Dalle-Donne, I., Rossi, R., Giustarini, D., Colombo, R., and Milzani, A. (2003) Actin S-glutathionylation: Evidence against a thiol-disulphide exchange mechanism. *Free Radical Biol. Med. 35*, 1185−1193.
(41) Wei, Q., Jiang, H., Xiao, Z., Baker, A., Young, M. R., Veenstra, T. D., and Colburn, N. H. (2008) Sulfiredoxin−Peroxiredoxin IV axis promotes human lung cancer progression through modulation of specific phosphokinase signaling. *PNAS 105*, 19738−19743.
(42) Briggs, M. W., and Sacks, D. B. (2003) IQGAP proteins are integral components of cytoskeletal regulation. *EMBO Rep. 4*, 571−574.
(43) White, C. D., Brown, M. D., and Sacks, D. B. (2009) IQGAPs in cancer: A family of scaffold proteins underlying tumorigenesis. *FEBS Lett. 583*, 1817−1824.
(44) Zhukova, L., Zhukov, I., Bal, W., and Wyslouch-Cieszynska, A. (2004) Redox modifications of the C-terminal cysteine residue cause structural changes in S100A1 and S100B proteins. *Biochim. Biophys. Acta 1742*, 191−201.
(45) Tarabykina, S., Scott, D. J., Herzyk, P., Hill, T. J., Tame, J. R., Kriajevska, M., Lafitte, D., Derrick, P. J., Dodson, G. G., Maitland, N. J., Lukanidin, E. M., and Bronstein, I. B. (2001) The dimerization interface of the metastasis-associated protein S100A4 (Mts1): In vivo and in vitro studies. *J. Biol. Chem. 276*, 24212−24222.
(46) Wood, Z. A., Poole, L. B., and Karplus, P. A. (2003) Peroxiredoxin evolution and the regulation of hydrogen peroxide signaling. *Science 300*, 650−653.
(47) Choi, M. H., Lee, I. K., Kim, G. W., Kim, B. U., Han, Y. H., Yu, D. Y., Park, H. S., Kim, K. Y., Lee, J. S., Choi, C., Bae, Y. S., Lee, B. I., Rhee, S. G., and Kang, S. W. (2005) Regulation of PDGF signalling and vascular remodelling by peroxiredoxin II. *Nature 435*, 347−353.
(48) Woo, H. A., Yim, S. H., Shin, D. H., Kang, D., Yu, D. Y., and Rhee, S. G. (2010) Inactivation of peroxiredoxin I by phosphorylation allows localized $H_2O_2$ accumulation for cell signaling. *Cell 140*, 517−528.